Prognostic Evaluation of Assumptions Used by Cumulus Parameterizations

GEORG A. GRELL*

*National Center for Atmospheric Research,** Boulder, Colorado*

(Manuscript received 2 May 1991, in final form 4 November 1991)

ABSTRACT

Using a spectral-type cumulus parameterization that includes moist downdrafts within a three-dimensional mesoscale model, various disparate closure assumptions are systematically tested within the generalized framework of dynamic control, static control, and feedback. Only one assumption at a time is changed and tested using a midlatitude environment of severe convection. A control run is presented, which shows good agreement with observations in many aspects. Results of the sensitivity tests are compared to observations in terms of sea level pressure, rainfall patterns, and domain-averaged bias errors (compared to the control run) of various properties.

The dynamic control is the part that determines the modulation of the convection by the environment. It is shown that rate of destabilization, as well as instantaneous stability, work well for the dynamic control. Integrated moisture convergence leads to underprediction of rainfall rates and subsequent degrading of the results in terms of movement and structure of the mesoscale convective system (MCS).

The feedback determines the modification of the environment by the convection, and in this study is considered together with the static control, which determines cloud properties. All feedback and static-control assumptions tested here seem very important for the prediction of sea level pressure and rainfall. The most crucial ones were downdrafts and lateral mixing.

As an interesting by-product, it is shown that a very simplistic and computationally highly efficient convective parameterization scheme leads to a very realistic simulation of the MCS, if the scheme uses a stability closure, assumes a large cloud size, parameterizes moist downdrafts, and does not assume unrealistically large lateral mixing.

1. Introduction

While the number of cumulus parameterizations continues to grow, few systematic tests have been made of their fundamental assumptions. Commonly, three different methods have been used to test parameterization schemes. These are termed diagnostic, semiprognostic, and fully prognostic. When testing diagnostically, one can observe the correlation between convective activity (measured in terms of rainfall) and various properties such as moisture convergence, instability, or destabilization. Although this will help identify relationships between reality and commonly used closure assumptions, which are used to determine the modulation of convection by the environment (the dynamic control), it cannot be used to verify a cumulus parameterization scheme as a whole, nor can it be used to quantitatively verify a part of a scheme. It can only give qualitative ideas about the applicability of various closure assumptions.

The semiprognostic approach (Lord 1982; Krishnamurti et al. 1980, 1983; Kuo and Anthes 1984; Grell et al. 1991) avoids the complexity of a fully prognostic model, yet tries to more rigorously test the parameterization schemes. Since a numerical weather prediction (NWP) model has a high level of complexity, it is difficult, if not impossible, to isolate the errors caused by cumulus parameterizations from errors caused by other components of the model (i.e., PBL parameterization, initialization, or numerical methods). The semiprognostic tests try to avoid these problems by diagnostically analyzing datasets (to determine heat and moisture budgets as residuals), and then using the datasets to make a one-time-step forecast with the cumulus parameterization scheme. Diagnostic heat and moisture budgets can then be compared to the "prognostic" results of the parameterization scheme. This is a good tool to identify errors and to estimate applicability limits and the validity of closure assumptions. Grell et al. (1991), hereafter referred to as GKP, using the semiprognostic tests with SESAME (Severe Environmental Storms and Mesoscale Experiment) data, found systematic errors in many parts of several parameterizations. Closure assumptions, such as pure instantaneous stability adjustments, produced erroneous rainfall pat-

* Current affiliation: NOAA/ERL Forecasts Systems Laboratory, Boulder, Colorado.

** The National Center for Atmospheric Research is sponsored by the National Science Foundation.

Corresponding author address: Dr. Georg A. Grell, NOAA/ERL FSL, 325 S. Broadway, Boulder, CO 80303.

terns. The vertical distribution of heating and drying rates was much affected by downdrafts (and anything that relates to them) as well as by lateral mixing. Since this type of test does not allow for any interaction beyond one time step, however, an absolute statement about the validity of assumptions cannot be given.

As a third choice, highly complex three-dimensional numerical weather prediction (NWP) models are run with one parameterization over an interesting time period. Then the experiment is repeated but with a different parameterization. Conclusions are often speculative because of the high complexity of the model. Furthermore, it might even be more guessing work to decide why one parameterization has failed and why another one was better. Parameterizations by themselves are very complex. In addition, results are quite often case dependent. While indeed some assumptions might be better for very specific environments or on specific scales, the test described above does not provide an answer to this problem either.

In this paper, we will try to compromise between the semiprognostic and the fully prognostic tests. We will try to apply results from previously performed semiprognostic tests (GKP) to a fully prognostic application, yet we will try to avoid switching a parameterization as a whole, instead concentrating on testing single, disparate assumptions. The main objectives include the development of a general framework for convective parameterizations with many degrees of freedom and much flexibility to change one assumption at a time, and, using this framework, the study of the effects of systematic errors—as identified in semiprognostic tests—on a fully prognostic forecast of a mesoscale convective system (MCS). We will not attempt to make an absolute statement about what parameterization is best as a whole, but rather will try to evaluate the validity of specific assumptions and the statistical effect they have on the numerical model.

Although a variety of test cases should be used, we will concentrate only on a well-studied case (which inhibits large sensitivity to small changes in the parameterizations and is highly convective). The test case chosen is a dataset from the PRE-STORM (Preliminary Regional Experiment for STORM-Central) from 10 June 1985.

In section 2, we will describe the numerical model and the dataset to be used. Section 3 will discuss the experimental design. We will explain how and what type of assumptions are changed, one at a time, within a generalized framework. Results will be shown in the fourth section, and conclusions will be given in the fifth section.

2. The numerical model and the dataset

The three-dimensional model used in this study is a nested-grid version of the Pennsylvania State University–National Center for Atmospheric Research (PSU–NCAR) hydrostatic mesoscale model (Anthes et al. 1987). The nested grid is two-way interactive, with grid spacings of 75 km for the coarse grid, 25 km for the nested grid, and 19 vertical sigma levels. Boundary conditions for the coarse domain are obtained by interpolating the 12-h observational analysis linearly in time according to Perkey and Kreitzberg (1976). This model setup is identical to the one described in Zhang et al. (1989). All runs use the full physical package, which includes a high-resolution Blackadar (1979) PBL parameterization, and both implicit and explicit formulation for precipitation physics. The explicit scheme includes predictive equations for cloud water and rainwater, as well as the effects of ice and snow (Zhang 1989). The coarse grid uses an Anthes–Kuo-type (Anthes et al. 1987) cumulus parameterization scheme. The spectral cumulus parameterization used for the nested domain is described in more detail in Grell (1988). This parameterization is based on Lord (1978), but moist convective-scale downdrafts have been included. Some details on the theoretical and numerical aspects of the inclusion of downdrafts, as well as other differences compared with Lord (1978), are given in the appendixes. This scheme was used extensively for semiprognostic tests in GKP, except that for the case following, the entrainment rate instead of the cloud-top height is used as the spectral parameter to characterize the cloud. For all the experiments hereafter (unless otherwise stated), up to six clouds are allowed in the spectrum.

The dataset selected for this study is taken from the 1985 PRE-STORM experiment and was provided by Dalin Zhang. It describes the evolution of an intense squall line on 10–11 June 1985. This dataset has been studied in detail (Rutledge et al. 1988; Johnson and Hamilton 1988; Zhang et al. 1989; Zhang and Gao 1989) and is well documented. In addition, Zhang et al. (1989) and Zhang and Gao (1989) used this dataset for three-dimensional model simulations with the Fritsch and Chappel (1980, hereafter FC) cumulus parameterization scheme and the same mesoscale model used in this study. Analyzed surface pressure fields and a cross section through the northern part of the squall line are shown in Fig. 1 for 0600 UTC 11 June (Johnson and Hamilton 1988). The surface analysis fields show the position of the mature squall line and the corresponding mesoscale pressure systems, including the mesohigh, the presquall low, and the wake low at 0300 UTC, which splits into two wake lows by 0600 UTC. The cross section (from Johnson and Hamilton 1988) depicts the position of the rear-inflow jet with respect to the northern wake low.

3. Description of the methodology

In this section, we will briefly describe the methodology. We will use the terminology of dynamic control, static control, and feedback in the same way as

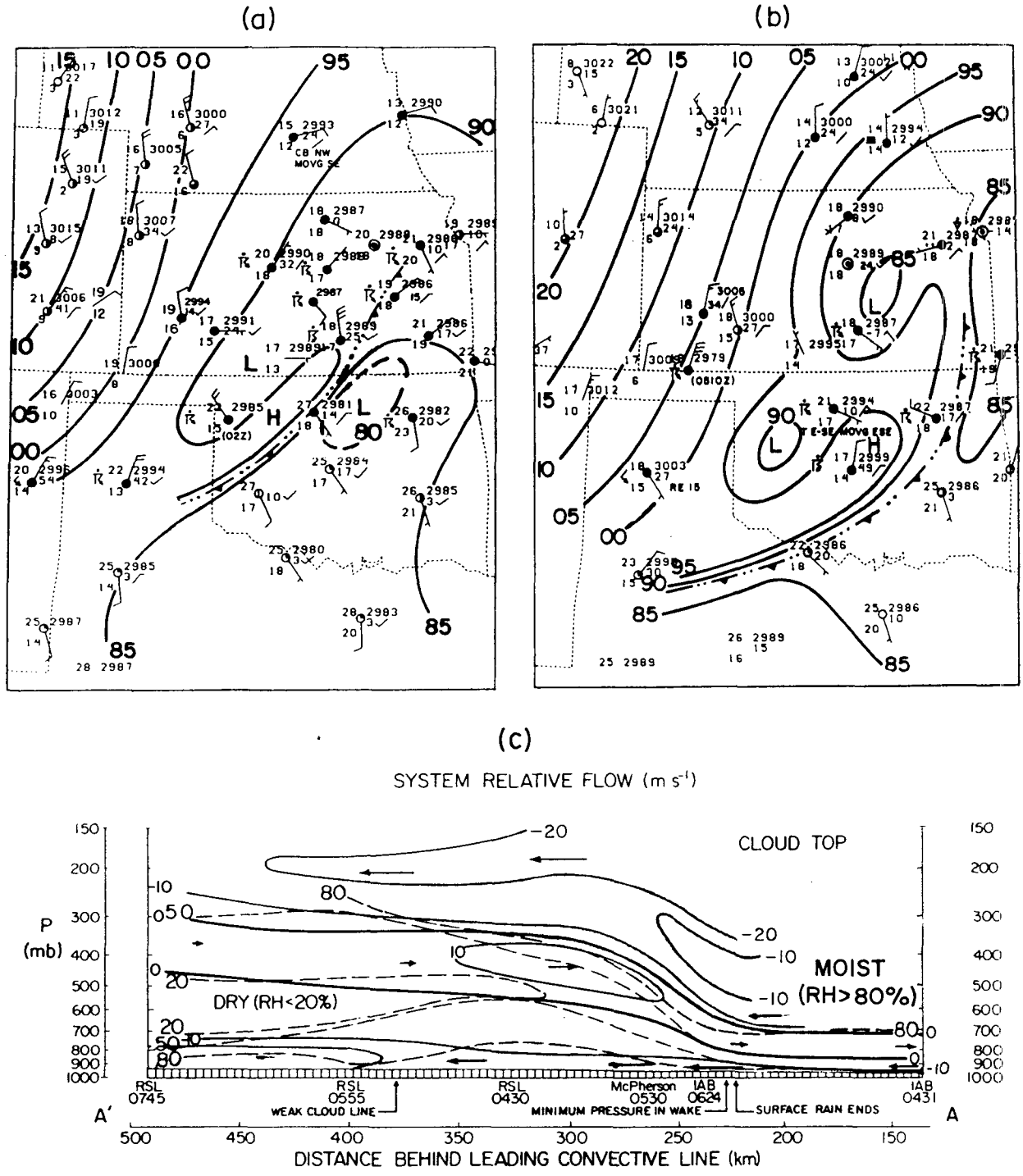

FIG. 1. Analyzed sea level pressure (from Johnson and Hamilton 1988) at 0300 UTC (a), 0600 UTC (b), and a cross section (c) through the squall line and the northern wake low at 0600 UTC, depicting system-relative flow and relative humidity (from Johnson and Hamilton 1988).

in GKP to systematically separate assumptions used in convective parameterizations. This terminology was originally introduced by Betts (1974). It splits cumulus parameterizations from the modeling point of view. The dynamic control determines the modulation of the convection by the environment. It must know where and how strong the convection will be. The feedback specifies the modification of the environment

by the convection. It distributes the total integrated heating and drying in the vertical. The static control determines the updraft or downdraft properties, and includes such mechanisms as entrainment, detrainment, and microphysics.

a. The dynamic control

Three commonly used assumptions for the dynamic control are based on environmental stability or moisture convergence. Examples of schemes using stability assumptions include the Arakawa and Schubert (1974, hereafter AS), FC, and Kreitzberg and Perkey (1976, hereafter KP) parameterizations. Stability closures assume that the observed change of the available buoyant energy is known. This observed change can be separated into changes by the larger scale and changes by the cumulus convection. We can therefore write (see also AS)

$$\frac{d\mathrm{AB_{tot}}}{dt} = \frac{d\mathrm{AB_{LS}}}{dt} + \frac{d\mathrm{AB_{CU}}}{dt}, \tag{3.1}$$

where AB is the available buoyant energy, subscript LS stands for larger scale, and subscript CU for cumulus convection. Arakawa and Schubert assume a quasi-equilibrium between the terms on the right-hand side of the equation; hence,

$$\frac{d\mathrm{AB_{tot}}}{dt} \approx 0. \tag{3.2}$$

This closure (the quasi-equilibrium assumption) is used in the control run (DQEQU). In a true quasi-equilibrium assumption, Eq. (3.2) cannot be solved exactly. One usually minimizes $d\mathrm{AB_{tot}}/dt$ with a linear programming method (Lord 1978). This is also done in all following experiments that use this closure assumption. Cumulus parameterizations in mesoscale models frequently assume

$$\left(\frac{d\mathrm{AB}}{dt}\right)_{\mathrm{CU}} = -\frac{\mathrm{AB}}{\Delta\tau}, \tag{3.3}$$

where $\Delta\tau$ is some specified time interval over which the instability is removed. Kreitzberg and Perkey use this type of closure, without any dependence on larger-scale motions. Here, we call this a pure instantaneous stability closure. Fritsch and Chappel use a similar closure. It is tested in experiment DFC. Note that this closure, as used in the experiments following, is purely predictive. It determines the amount of convection as well as the size of the convective elements. This is in contrast to the implementation of an instantaneous stability closure in FC or KP. All of the experiments hereafter will use the purely predictive scheme, which selects the cloud sizes internally. The only exception is described in section 3c. Although an experiment with a pure instantaneous stability closure (KP) has also been performed, results were almost identical to experiment DFC and are not shown here.

A second type of closure makes use of the observation that the convective activity is closely related to the total moisture convergence (Charney and Eliassen 1964; Kuo 1965, 1974; Anthes 1977) or the integrated vertical advection of moisture (Krishnamurti et al. 1980, 1983; Molinari 1982, 1985). In most of these schemes the drying is limited to the amount of integrated moisture convergence, or the integrated vertical advection of moisture. Fritsch et al. (1976) and GKP, using very different datasets, have shown that the moisture convergence is usually not sufficient on synoptic scales to explain the rainfall rates. It seemed necessary to allow for a negative moistening parameter b, or a closure for additional—supposedly unresolved—mesoscale moisture convergence as proposed by Krishnamurti et al. (1983). In experiment DKUO, to simulate the effect of the restriction of the rainfall rates in Kuo-type schemes, we let the regular cumulus parameterization determine the rainfall and feedback (if integrated vertical advection of moisture is positive), but scale the total rainfall rate R with a proportionality factor $\alpha_r(x, y, t)$ (which is a function of time and space, but not of cloud type) in accordance with

$$\alpha_r(x, y, t)(R)_{\mathrm{QEQU}} = (R)_{\mathrm{DKUO}} = -\int \omega \frac{\partial q}{\partial p}\, dp, \tag{3.4}$$

so that the total rainfall rate will equal the integrated vertical advection of moisture. Here, ω is the vertical velocity in pressure p coordinates and q is the specific humidity. Since in the cumulus parameterization used here all feedback equations have a linear dependence on the normalized cloud-base mass flux m_b (see also appendix A), α_r can readily be used in the calculation of the feedback.

Recently Frank and Cohen (1987) employed a different idea by introducing a downdraft forcing into the dynamic control. Their dynamic control is based on low-level mass-flux convergence. The downdrafts will cause additional mass-flux convergence, creating subsequent forcing of more convection. This represents a physically realistic idea and could be implemented in Eqs. (1) or (3). Furthermore, it can be a realistic physical interpretation for the closure used by Krishnamurti et al. (1983) (to explain the necessary additional unresolved moisture convergence). The study of this particular aspect, however, is beyond the scope of this paper. Various moisture convergence closures will be studied in more detail in a subsequent paper.

b. Feedback and static control

Historically, there are many disparate approaches to parameterizing the modification of the environment by convection. The first type is used by some of the Kuo-type schemes (Kuo 1974; Krishnamurti et al. 1980, 1983; Molinari 1982). This approach envisions that the convection will tend to adjust the atmosphere toward a moist neutral state. The feedback then is sim-

ply dependent on temperature and moisture differences between the cloud and the environment. Other Kuo-type schemes (Anthes 1977; Donner 1993) try to estimate the vertical eddy-flux term and the condensation by using a one-dimensional cloud model. As in the feedback discussed next, this approach means that the convective effects are being caused by subsidence and detrainment (Grell 1988), if the assumed clouds have a steady-state character.

Another approach assumes that the convective clouds have a purely steady-state character (AS). Consequently, convection influences the environment through subsidence and detrainment at the top of the updraft or the downdraft (if downdrafts are parameterized). Detrainment around the cloud edges may also be included. Note that for this approach, it is not important where (at what level) the latent heat release in the cloud actually occurs, except where it influences the magnitude of the cloud mass flux.

A third approach was originally introduced by Fraederich (1973) and is also used by KP and FC. It assumes a cloud rises and then instantly decays. Thus, after subsidence calculations, the convection is supposed to build and decay without a steady-state stage, and the cloud properties are mixed horizontally with the subsided environment. A separation into even more approaches can then be achieved by envisioning clouds with or without downdrafts. Since some of these feedback mechanisms depend strongly on the static control (entrainment, detrainment, downdraft properties, microphysics of cloud model), we have constructed the following set of experiments.

In experiments FDD0, FDD1, and FDDS we will test the sensitivity to the downdraft by removing it completely (FDD0), weakening it (FDD1), and keeping it stronger (FDDS). The "tuning" can be achieved in different ways. The downdraft mass flux in the parameterization used in this study depends strongly on the precipitation efficiency β or on the entrainment rate λ. Increasing entrainment into the downdraft slightly, or decreasing the precipitation efficiency, will both increase the mass flux. Since results from either experiment were very similar to each other, we will show only experiments where we linearly decreased the precipitation efficiency (FDDS) by 10%, and increased it (FDD1) by 10%. In experiment FLM, to simulate a lateral mixing effect, detrainment around the clouds is assumed to equal the entrainment. Although the detrainment rates could be variable, as in Kain and Fritsch (1990), the more simplistic approach was chosen for the scope of this paper.

c. *Simplifying the spectrum and the interaction between clouds: A simple one-cloud scheme*

GKP showed that a modified version of the AS scheme was very insensitive to parameters such as entrainment or detrainment. They found that weak or no downdrafts, non-mass-flux-type feedbacks, and some of the dynamic-control closure assumptions led to large errors. Here, in experiment DONE, we will show that a very simple and highly efficient parameterization, which tries to avoid these errors, may do as well as the very sophisticated scheme. We will cut the cloud spectrum to just one extremely simple nonentraining cloud (updraft and downdraft couplet). This means that we will prescribe the cloud size as in other parameterizations (FC, KP). The dynamic control will not determine the spectrum of clouds but only the amount and location of convection. Equation (3.2) does not require a linear programming method, and has an exact solution. Even in its most complicated form (using large-scale destabilization for the dynamic control), with the use of the discretized version of this spectral cumulus parameterization scheme described in appendix B, this scheme becomes very efficient. All terms dependent on entrainment or detrainment are zero, the normalized mass flux is constant with height ($=1$), the cloud work functions for updraft and downdraft simply become the available buoyant energy for updraft and downdraft, respectively. The calculations become even more simple if moisture convergence or instantaneous stability is used as the closure in the dynamic control. All experiments are summarized in Table 1.

4. Results

Figure 2 shows the simulated sea level pressure field and streamlines at 18 h (0600 UTC), as forecast by experiment DQEQU. Similar to Zhang et al. (1989), this run simulates the sea level pressure fields remarkably well. The generation of the presquall mesolow, the squall-line mesohigh, and the two wake lows is captured by the model simulation (compare with observations shown in Fig. 1). Note the exceptionally good prediction of the position and intensity of the two wake lows at 0600 UTC in Oklahoma and Kansas. Keep in mind that only conventional data were used to initialize the model, yet it was able to generate the meso-β-scale features in this 18-h prediction. The hourly rainfall rates averaged around 0000, 0300, and 0600 UTC (Fig. 2) illustrate the position of the mesoscale pressure systems with respect to the evolution of the squall line. The rear-inflow jet is also simulated well (a cross section showing the flow normal to the squall line, and through the northern wake low is shown in Fig. 3). The magnitude of the jet is probably a little too strong. Consequently, the wake low is a little intense. Although some of the following experiments have a similarly good simulation (some might even be better), we will use results from the experiment DQEQU as a control run. Note that this does not mean that for this case this particular version of the parameterization is the best choice (as will be shown later), but rather that it is an acceptable choice. As indicated

TABLE 1. List of experiments. The control run is denoted by DQEQU. Only one assumption at a time is altered (except for experiment DONE). The table indicates the varied assumption within the framework of dynamic control, static control, and feedback for the particular experiment.

Experiment name	Dynamic control	Feedback and static control	
DQEQU	quasi-equilibrium assumption		$\left(\frac{d\mathrm{AB}}{dt}\right)_{\mathrm{tot}} \approx 0$
DFC	instantaneous stability		$\left(\frac{d\mathrm{AB}}{dt}\right)_{\mathrm{Cu}} = -\frac{\mathrm{AB}}{\Delta\tau}$
DKUO	moisture convergence		$R = -\int \omega \frac{\partial q}{\partial p}\, dp$
FDD0		no downdrafts	$\beta(i) = 0$
FDD1		weaker downdrafts	$\beta(i) = \beta(i) - 0.1$
FDDS		stronger downdrafts	$\beta(i) = \beta(i) + 0.1$
FLM		strong lateral mixing	$\lambda_d(i) = \lambda_e(i)$
DONE	rate of destabilization	downdrafts no lateral mixing	see section 3c

by GKP, however, the quasi-equilibrium assumption seems valid for mesoscale applications, even in summertime convective situations.

Figure 4 shows sea level pressure fields and streamlines at 0600 UTC as predicted by experiments DFC and DKUO. While for the FC closure results are very similar to experiment DQEQU, a significant difference is noted for the moisture-convergence closure used in DKUO. In experiment DKUO, the mesoscale pressure systems were not simulated properly. The southern wake low is almost nonexistent, and the mesoscale high pressure system covers too large of an area. Note that the only difference between DQEQU and DKUO is that the amount of convection has been scaled down or up to make the rainfall rate fit the integrated vertical advection of moisture. Figure 5 shows the rainfall rates at 0000, 0300, 0600 UTC, and the total accumulated rainfall (convective and nonconvective) for experiment DKUO. Here, the differences become obvious. Much less total rain is produced. Most of this was caused by the underprediction of the rainfall rates (almost no rain is predicted) during the first 12 h. This rain was largely caused by a mesoscale convective complex (MCC) over eastern Kansas. Integrated moisture convergence was not sufficient to simulate the proper rainfall rates. A similar behavior was shown to apply for larger scales by Fritsch et al. (1976), as well as by GKP. While the movement of the squall line is simulated reasonably well for DKUO, the structure again shows some deficiencies. The mesoscale high pressure system is too intense, the wake lows almost nonexistent. The rainfall patterns indicate a wider and less-defined squall line. Although the underprediction of the rainfall rates does not come as a surprise, the important influence that this would have on the prediction of the mesoscale weather systems was a little unexpected.

Figure 6 shows domain-averaged bias errors (compared to DQEQU) for temperature and moisture at some selected levels, and for experiments DFC and DKUO. This figure supports the observation that the DKUO closure led to less convection, while the DFC closure led to more convection. Experiment DFC caused more cooling in low levels, warming in upper levels, and more overall drying. Note, however, that a DFC-type closure strongly depends on the choice of $\Delta\tau$ in Eq. (3), which for this case was chosen to be 20 min. Experiments with a pure instantaneous stability closure as in KP led to almost identical results for this case. Experiment DKUO gave significantly less drying over the first 12 h (the time when the MCC over eastern Kansas and Oklahoma was most active), with less cooling at the surface and less heating in the upper levels (Fig. 6b).

Figure 7 compares domain-averaged bias errors for moisture (shown are errors at selected levels as well as total integrated values) for experiments FDD0, FDD1, and FDDS. Quantitatively, the strongest effect of the downdraft is achieved in the lower troposphere, where drying and heating is much decreased. Note that this effect is more intense than the cooling in the surface layers. Interestingly, as the downdraft strength is increased further, there is a difference in model sensitivity depending on the type of MCS. While for the MCC the drying is decreased, for the squall line, the drying is increased. This points toward the increased importance of the parameterized downdraft cooling on the simulated squall-line dynamics. For the MCC, most of the simulated rain is convective. The model resolution is not sufficient to allow a large part of the MCC area to become saturated. As a consequence, increasing the downdraft strength in the parameterization (through decreasing the precipitation efficiency) will decrease the rainfall directly. The possible increase in dynamical forcing in the fairly weak wind shear—since the downdrafts have been artificially increased, causing additional convergence and overrunning—is too weak to offset this decrease in total rainfall intensity.

The sea level pressure fields and streamlines (Fig. 8) clearly show the importance of the downdrafts in the static control and feedback. Without downdrafts,

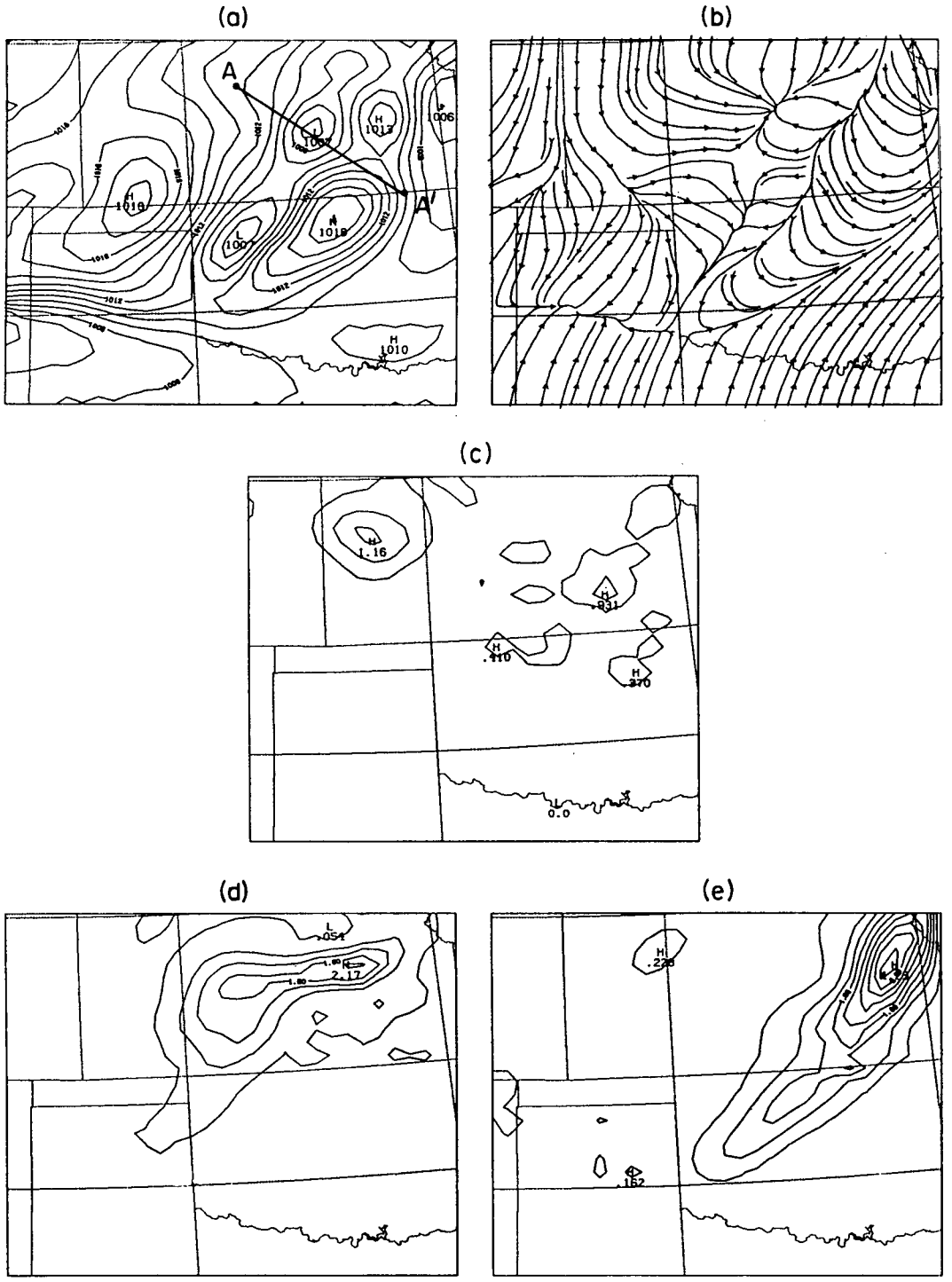

FIG. 2. (a) Simulated sea level pressure field and (b) streamlines at 0600 UTC. Also shown are 1-h rainfall accumulation (cm) at (c) 0000 UTC, (d) 0300 UTC, (e) 0600 UTC, and location (a) of cross section from Fig. 3. Contour interval is 1 mb for the sea level pressure fields, and 5 mm for the rainfall fields, with the lowest contour at 1 mm.

there is no resemblance of the mesoscale pressure systems to reality, and the squall line moves much slower. In fact, the squall line is almost nonexistent (see also Fig. 9 for a comparison of the rainfall fields). A decrease in downdraft mass flux of only 10% (FDD1) still significantly degrades the simulation. On the other hand, more intense downdrafts do not change the simulation significantly. For the simulation without the down-

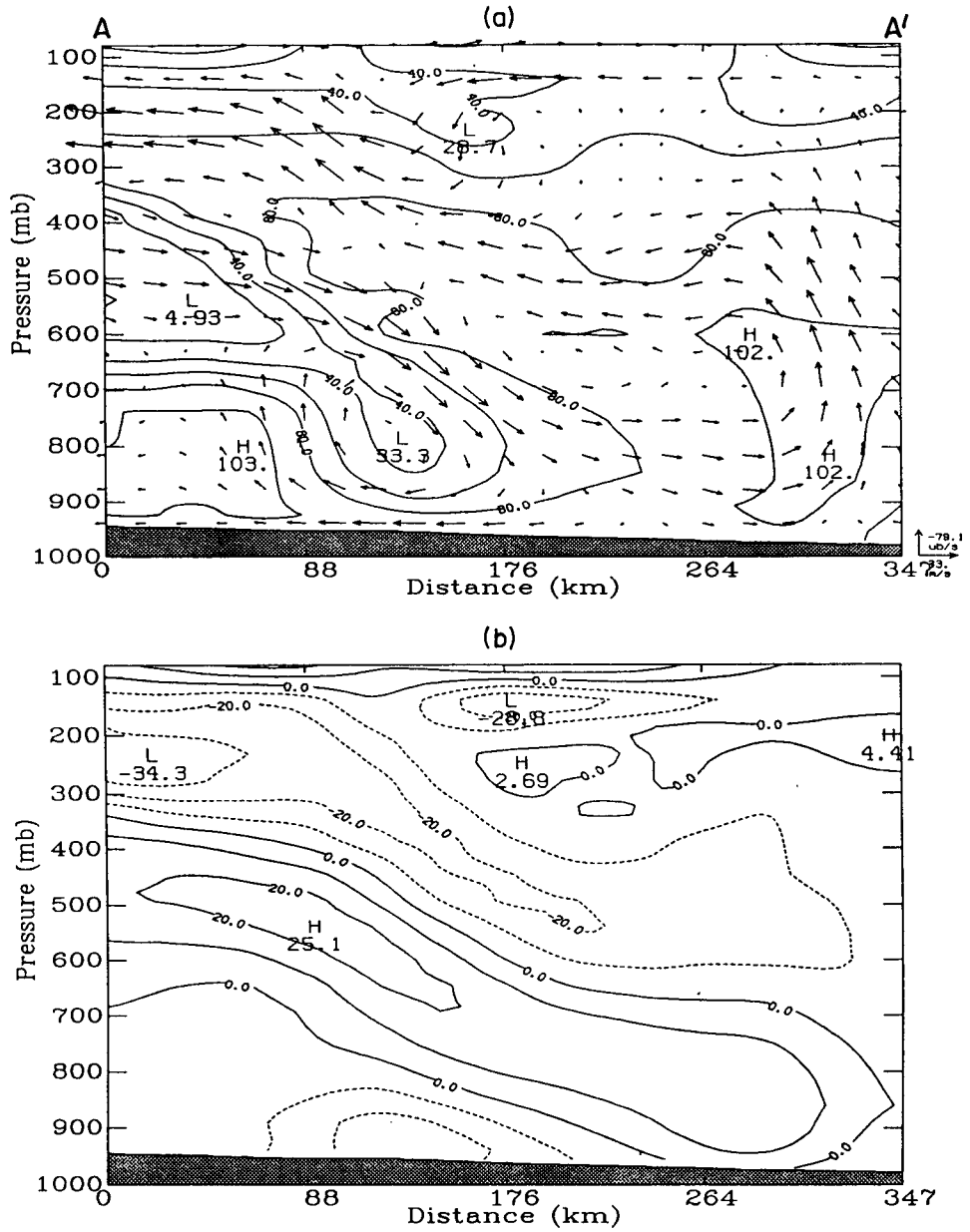

FIG. 3. Cross section through simulated squall line at 0600 UTC, depicting (a) system-relative flow and relative humidity, and (b) speed of system-relative flow. Units for the system-relative flow are in meters per second, with contours every 10 m s^{-1}. Contour interval for the relative humidity is 20%. Location of cross section shown in Fig. 2a (approximately as in Johnson and Hamilton 1988).

drafts (FDD0), almost all rain is convective. The intense heating and drying by this mass-flux-type scheme in the low levels (through subsidence) is hindering the explicit moisture scheme from becoming active (remember that the explicit scheme needs saturation to become involved), leading to large errors in this simulation. This should be expected, especially with this type of feedback, which assumes all the subsidence occurs inside the grid area. This must—on a 25-km scale—lead to large errors, if the subsidence heating and drying are overestimated. Note that the best simulation may be the one with the strongest downdrafts, where the squall line propagates much faster.

Here, it is interesting to note results from a supporting experiment, which is not described in detail. As a simple test of how important the parameterized downdraft cooling was for the simulation, we removed the downdraft cooling by setting the downdraft detrainment in the parameterization to zero. Note that this is not mass consistent. Furthermore, this does not

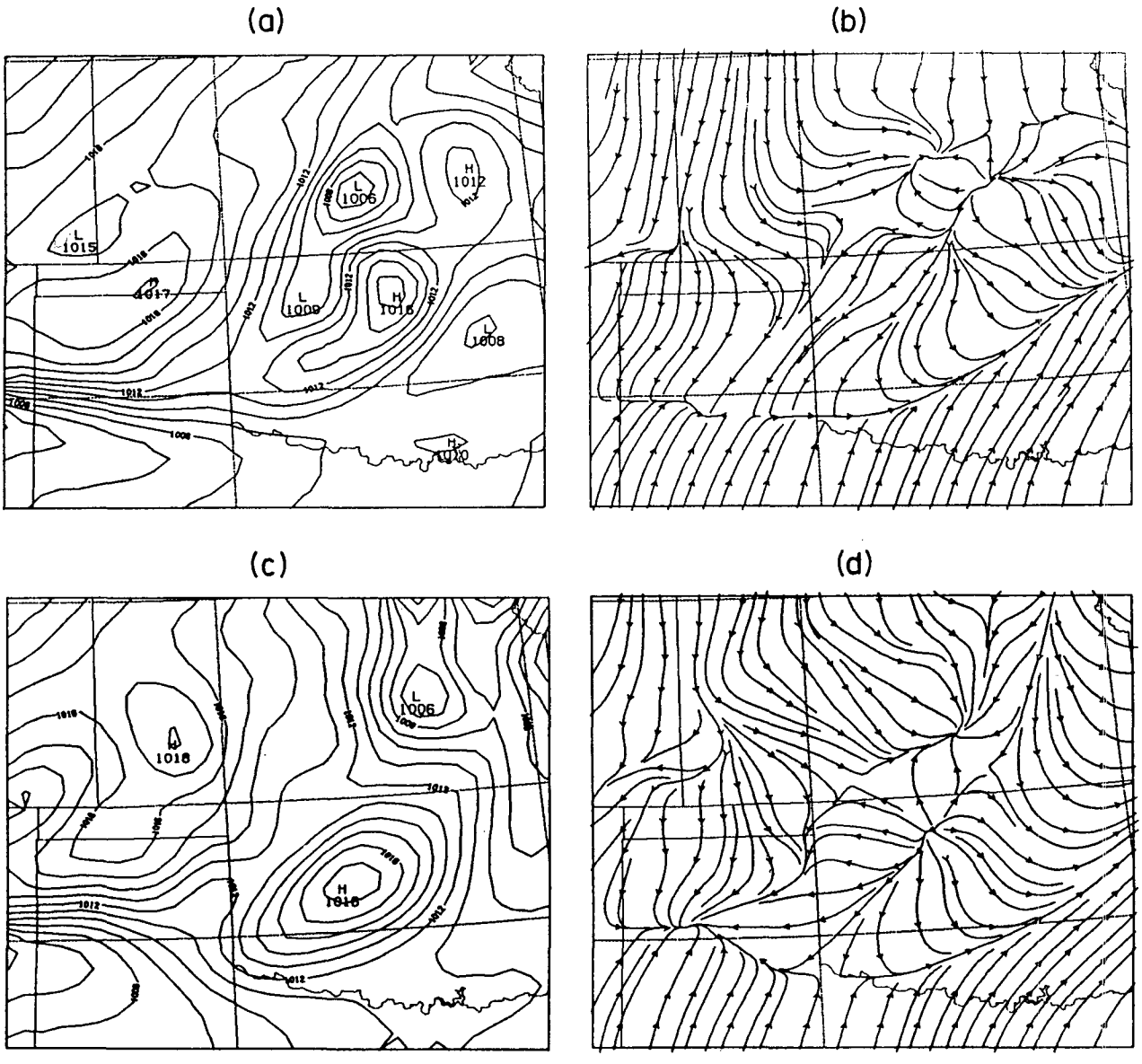

FIG. 4. Sea level pressure fields [(a) and (c)] and streamlines [(b) and (d)] at 0600 UTC for experiments DFC [(a) and (b)] and DKUO [(c) and (d)]. Contour interval is 1 mb for the sea level pressure fields.

by any means imply a conclusion as to whether the downdraft cooling in the real atmosphere is of importance. It is only a test of the parameterized part of the cooling for this case study. Nevertheless, the results were interesting. They indicated that the parameterized downdrafts were not the essential mechanism for creation of the mesoscale pressure systems. The cooling, however, seemed of some importance for the evolution of the squall line. It was clearly less well defined (a bit broader), and moved more slowly. While for a large-scale parameterization, for computational reasons, it might suffice to avoid the overprediction of the heating and drying in lower levels (maybe by introducing some sort of downdraft mechanism), a parameterization for mesoscale applications must do better than that.

Figure 10 shows some results from experiment FLM. Sea level pressure fields, streamlines, rainfall patterns, and total accumulated rain again indicate the importance of feedback assumptions. Lateral mixing clearly degrades the results in this case, where large detrainment rates were used. The quick moistening and warming by the mixing led to rapid switch off of the convective scheme, especially over the first 12 h in eastern Kansas. Almost all rain in the squall line is explicitly resolved, and the MCS moves much slower. It is also less well defined. It should be noted here that only substantial mixing of environmental air with updraft air can cause these problems. Results from runs with smaller detrainment rates, which are not shown here, led to almost identical results as in the control

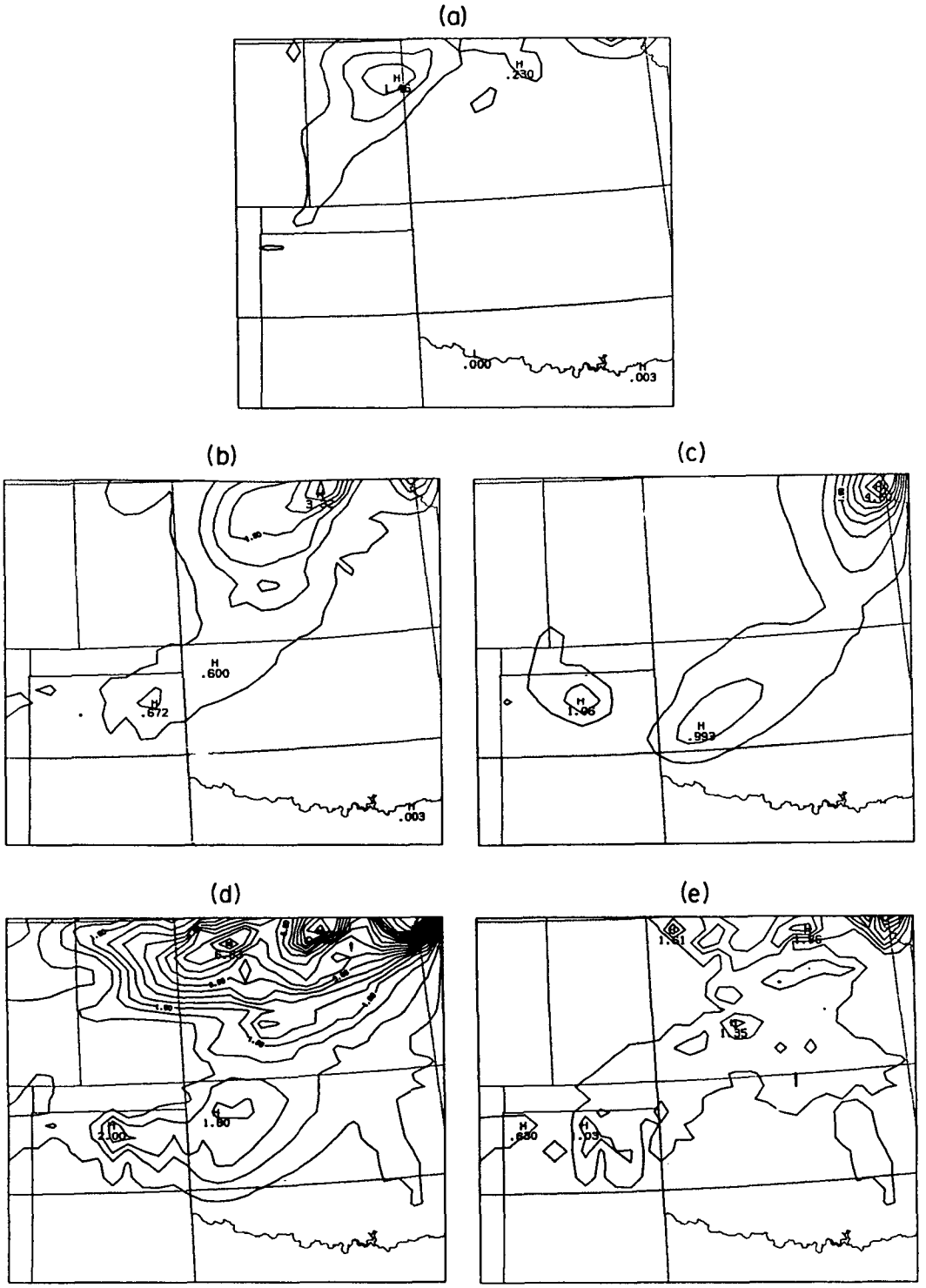

FIG. 5. (a)–(c) One-hour rainfall accumulations, (d) total rainfall accumulations (cm) over 18 h, and (e) total convective rainfall accumulations for experiment DKUO. Contour interval is 5 mm; the lowest contour is 1 mm.

run. This should be expected. GKP have shown that the mixing of very warm and moist updraft air with the environment can lead to large errors on larger-scale averages. There is no a priori reason why a parcel with 5° or more of temperature excess should stop ascending and instantly mix with the environment. Assuming more reasonable mixing rates, or assuming that the air that mixes with the environment has much less tem-

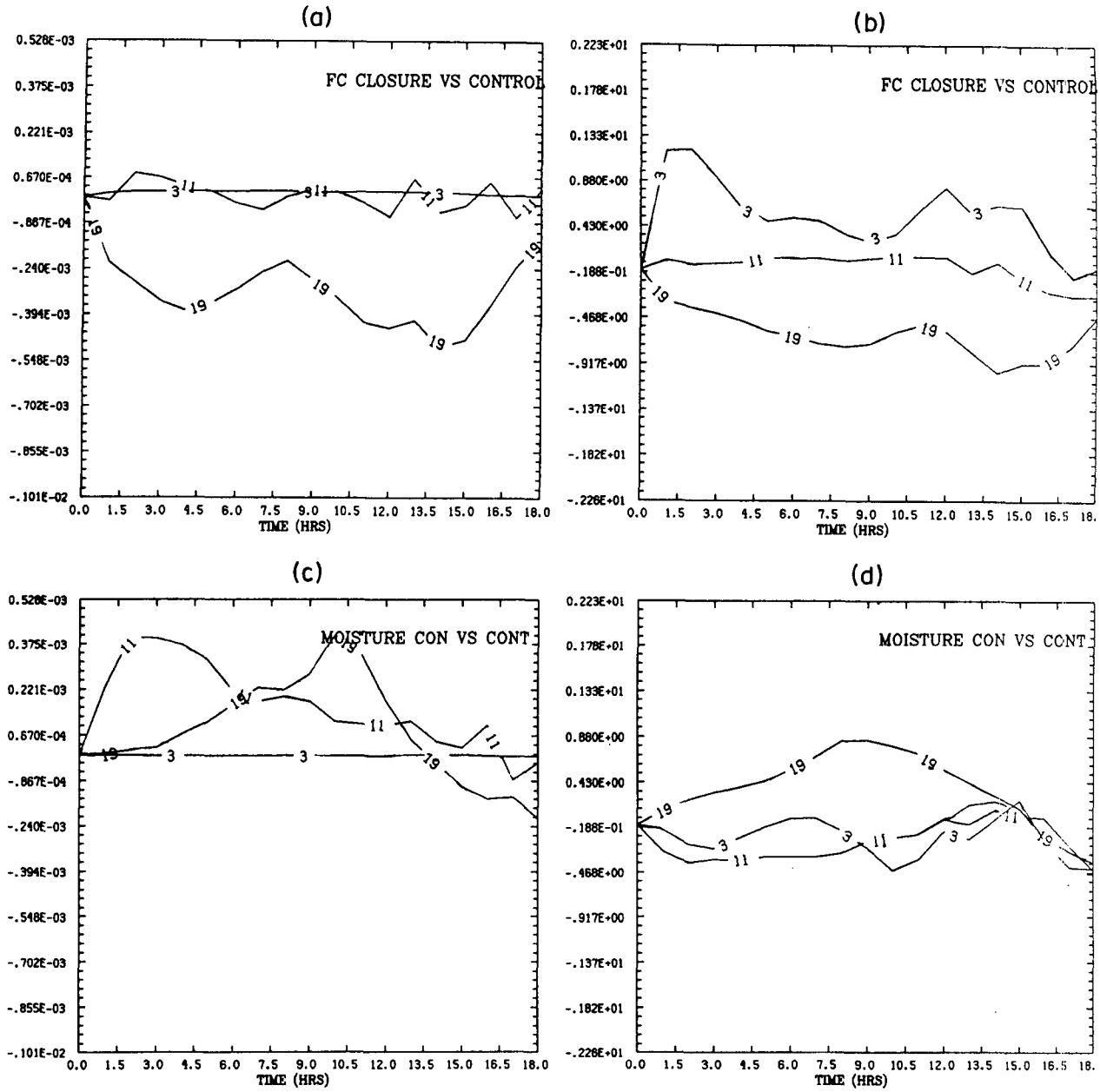

FIG. 6. Time section of domain-averaged bias errors of specific humidity [(a) and (c)], and temperature [(b) and (d)] at three sigma levels [$\sigma = 0.125$ (3), $\sigma = 0.5705$ (11), $\sigma = 0.9985$ (19)] and experiments DFC [(a) and (b)], and DKUO [(c) and (d)] versus the control run. Units are kilograms per kilogram for specific humidity and degrees Celsius for temperature.

perature or moisture excess, will lead to similar results as in the control run. Cloud models that would probably avoid these problems in the feedback were proposed by Taylor and Baker (1987) and Kain and Fritsch (1990).

Next, we will briefly look at the results of the simulation with the very simplistic one-cloud scheme described in section 3. This scheme avoids overprediction of the subsidence heating, uses a stability closure, and has intense downdrafts. Figure 11 shows the sea level pressure fields and streamlines at hour 18, and the rainfall rates at 0000, 0300, and 0600 UTC. Again, the simulation shows remarkable resemblance to reality. The position of the squall line may even be a little better for this run than for the control run (faster movement for experiment DONE). "Tuning" of the downdraft strength would in this case bring the simulation to even closer agreement (results not shown here) with run FDDS. This is a rather gratifying result. It indicates that, for mesoscale applications, it seems

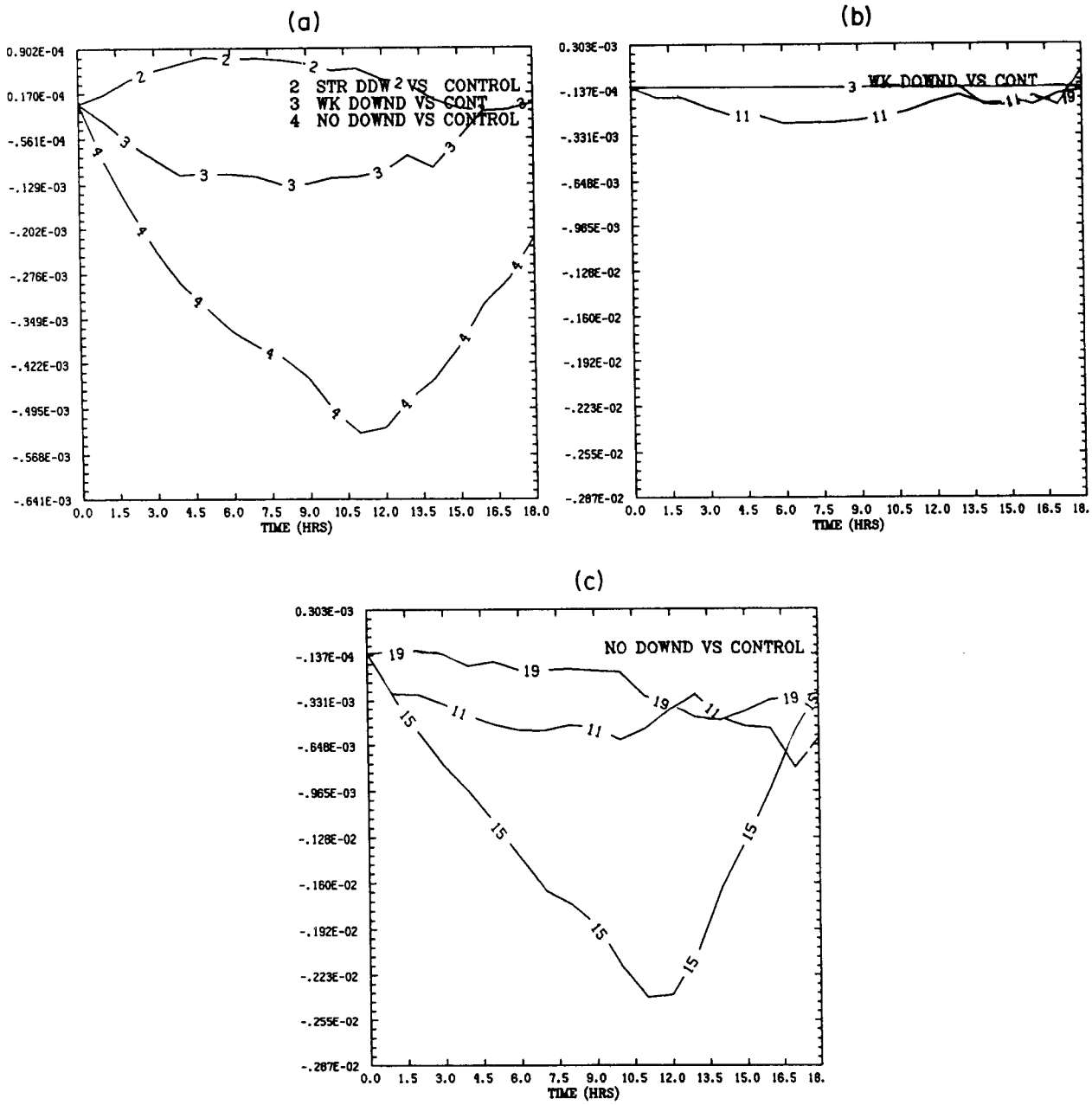

FIG. 7. Time section of domain-averaged bias errors of specific humidity at various [(b) and (c)] sigma levels [$\sigma = 0.125$ (3), $\sigma = 0.5705$ (11), $\sigma = 0.817$ (15), $\sigma = 0.9985$ (19)] and volume-averaged (a) bias errors for experiments FDD0 [(a) and (c)], FDD1 [(a) and (b)], and FDDS [panel (a)] versus the control run. Units are kilograms per kilogram.

to make almost no difference whether a spectrum of clouds is given out of which the dynamic control determines the cloud size by itself, or whether a cloud size of a large cloud is prescribed as in FC or KP. We have tried different cloud sizes for this experiment but found almost no differences in simulations as long as the clouds were assumed to be tall (entrainment rates corresponding to radius of more than 3 km; see also GKP). Computational costs are minimal for this type of scheme.

5. Conclusions

Zhang et al. (1989) have already indicated the importance of good physical packages, such as explicit treatment of cloud water, rainwater, snow, and ice. Furthermore, they have shown the importance of having both explicit, as well as implicit, treatments of convection. The results presented earlier agree with those findings. As a matter of fact, the timing of when the explicit and when the implicit schemes are active is

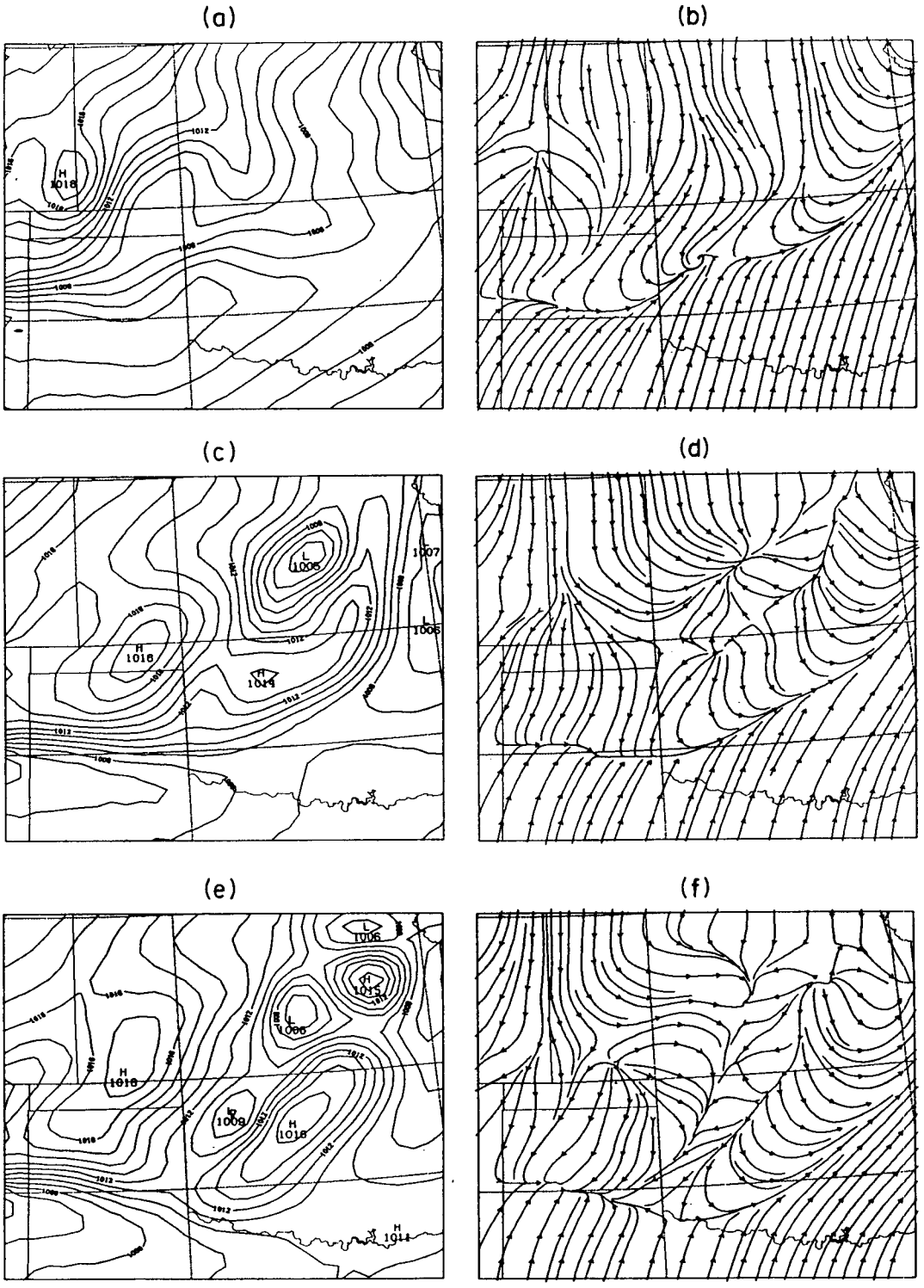

FIG. 8. Sea level pressure fields [(a), (c), and (e)] and streamlines [(b), (d), and (f)] at 0600 UTC for experiments FDD0 [(a) and (b)], FDD1 [(c) and (d)], and FDDS [(e) and (f)]. Contour interval is 1 mb for the sea level pressure fields.

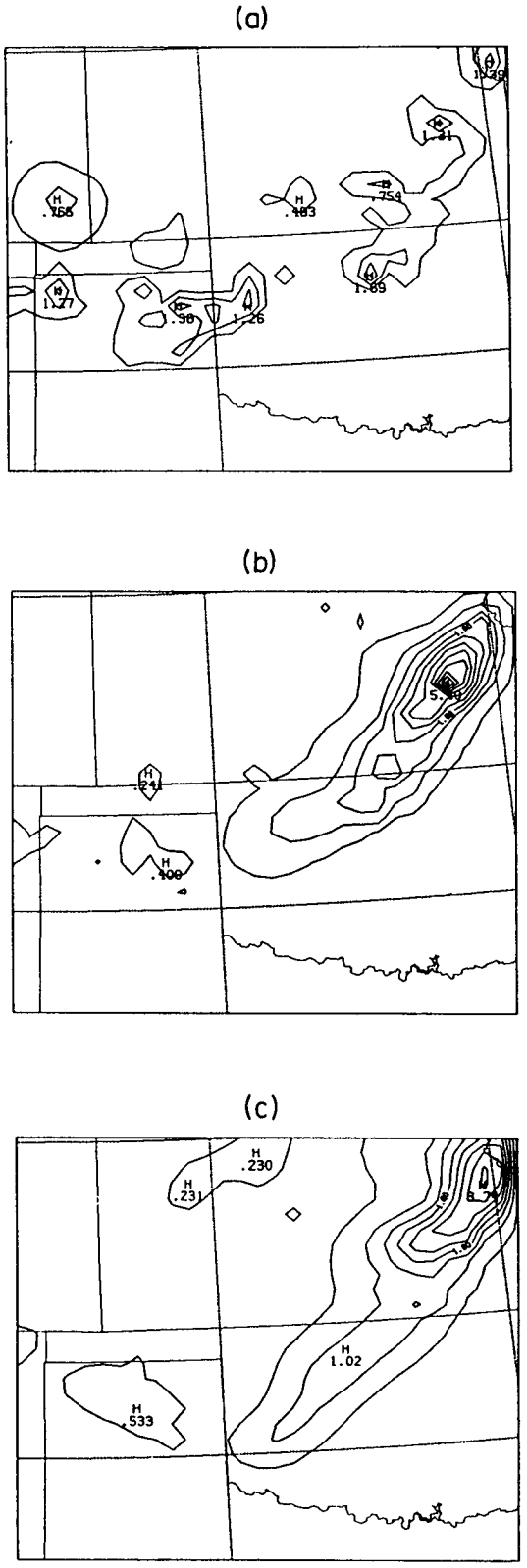

FIG. 9. (a)–(c) One-hour rainfall accumulations at 0600 UTC for experiments FDD0 (a), FDD1 (b), and FDDS (c) in centimeters. Contour interval is 5 mm; the lowest contour is 1 mm.

very important in these scales. Many of the dependencies of the simulations to parameterization assumptions can be explained in terms of this timing. Specifically, we have shown the following:

1) As estimated in the semiprognostic tests, the quasi-equilibrium assumption, which relates the strength and the location of the convection to the larger-scale destabilization, is valid for summertime midlatitude mesoscale applications.

2) In contrast to the semiprognostic tests, the use of instantaneous stability as a closure in the dynamic control of a cumulus parameterization scheme did not lead to significant errors or improvements in the model simulation. This should be expected, since in a three-dimensional model simulation large amounts of available buoyant energy will develop in areas with intense larger-scale destabilization. It came as a surprise, however, that no time lag between the two forecasts could be detected.

3) Integrated vertical advection of moisture as a closure led to underprediction of the rainfall rates. The adequate prediction of the rainfall rates was important for this particular case. Results using this type of moisture convergence closure were significantly degraded.

4) Feedback assumptions are very important in the midlatitude environment, especially on the mesoscale. When simulating this scale, the timing when the explicit moisture scheme kicks in becomes extremely important. As in the semiprognostic tests, overprediction of heating and drying in the lower troposphere introduces large noncorrectable errors. The explicit scheme does not kick in at the proper time (if at all). If the lateral mixing is too strong, the convection is too weak in the beginning of the simulation, and the explicit scheme has to carry the whole burden. In this case, the movement of the squall line was much too slow.

5) An Arakawa–Schubert-type spectral parameterization performed well in the high-resolution simulation of a midlatitude MCS if moist convective scale downdrafts are included in the cumulus parameterization and good physical packages are included in the three-dimensional NWP model. Such physical packages include a high-resolution planetary boundary layer parameterization and an explicit treatment of cloud water, rainwater, ice, and snow rather than just a removal of supersaturation.

6) A very simplistic and highly efficient cumulus parameterization scheme, which avoids the aforementioned problems, also leads to an excellent simulation of the squall line. Although this type of scheme is rather dull for research applications in the cumulus parameterization problem, it could be of much help for operational models.

Since only one dataset was used in this study, the conclusions have to be somewhat tentative. Current work is in progress to support the above findings with other datasets, as well as to study the importance of

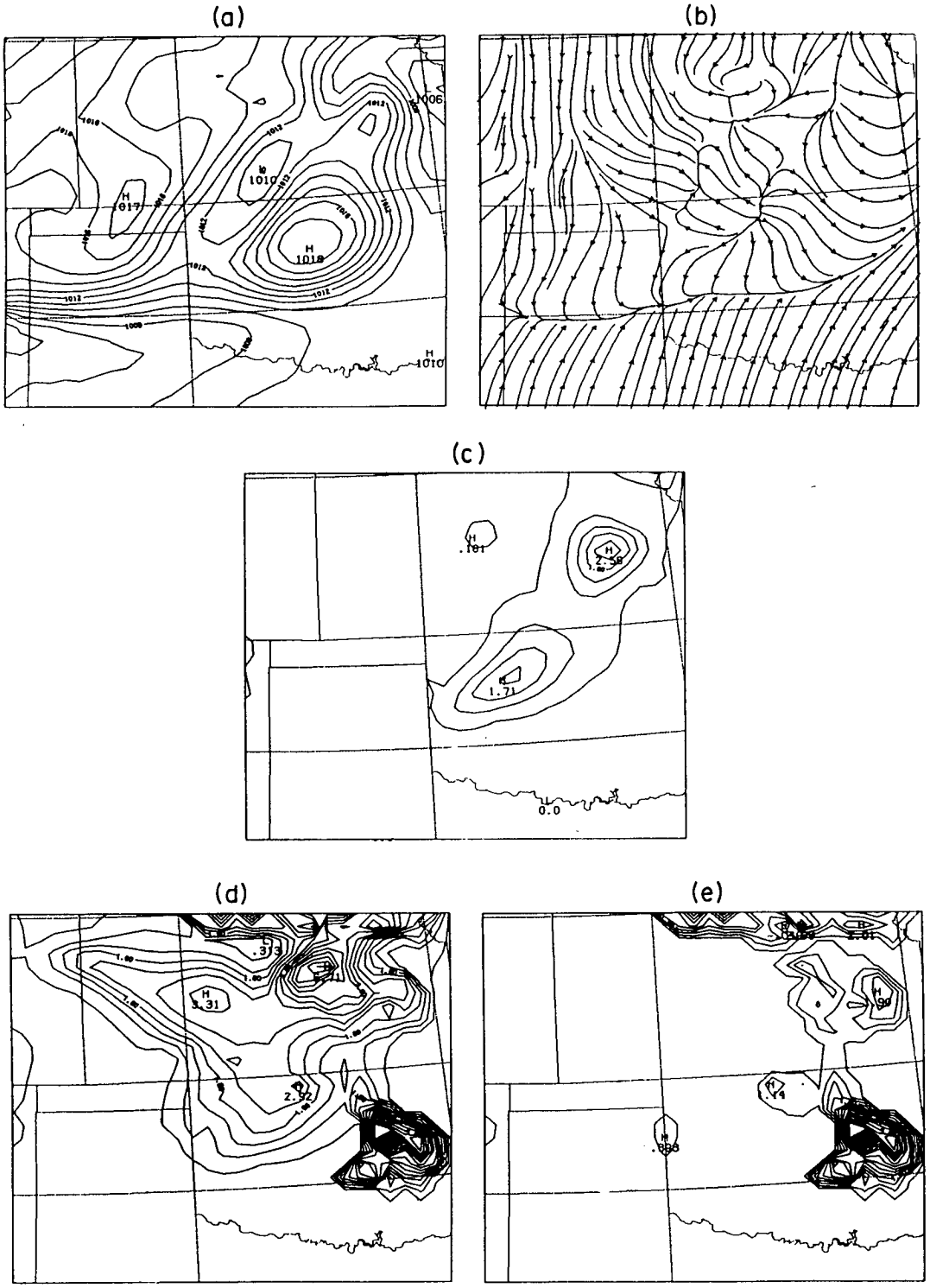

FIG. 10. (a) Sea level pressure field and (b) streamlines at 0600 UTC for experiment FLM. Also shown is (c) the 1-h rainfall accumulation, (d) the total rainfall accumulation over 18 h, and (e) the total convective rainfall accumulation for experiment FLM in centimeters. Contour interval is 1 mb for the sea level pressure fields, and 5 mm for the rainfall fields, with the lowest contour at 1 mm.

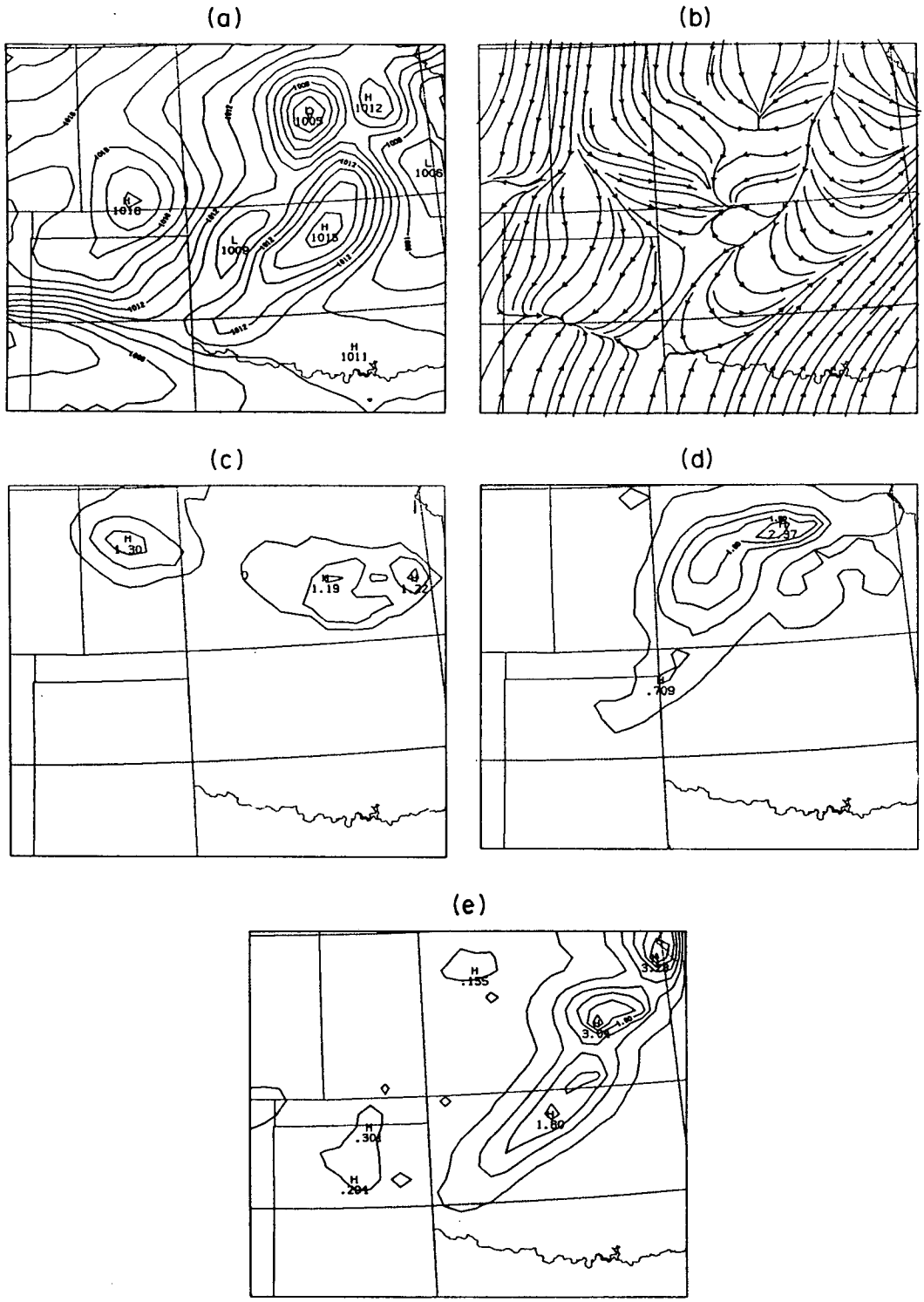

FIG. 11. (a) Simulated sea level pressure field and (b) streamlines for experiment DONE at 0600 UTC. Also shown for the same experiment are 1-h rainfall accumulation (cm) at (c) 0000 UTC, (d) 0300 UTC, and (e) 0600 UTC. Contour interval is 1 mb for the sea level pressure fields, and 5 mm for the rainfall fields, with the lowest contour at 1 mm.

shallow convection, and the many moisture-convergence closures.

Acknowledgments. I am grateful to Da-Lin Zhang and Kun Gao for supplying the dataset and valuable discussions. I also acknowledge Ying-Hwa Kuo for reviewing the manuscript, as well as for providing other valuable discussions. The constructive reviews of three anonymous reviewers also improved the quality of the paper significantly. Furthermore, I thank Evelyn Donall for editorial support, and the Mesoscale and Microscale Meteorology Division of NCAR for the computer support for this study. This work was supported by the Office of Naval Research under Grant N-00014-87-K-160, 100008.

APPENDIX A

The Parameterization of Moist Downdrafts

This appendix describes the inclusion of moist downdrafts into the equations of dynamic control, static control, and feedback used in the parameterization discussed earlier. They are taken from Grell (1988). Differences from the original AS scheme as described by Lord (1978) are pointed out.

a. Static control

All commonly used one-dimensional steady-state cloud models (plumes, bubbles, or jets) make use of the assumption that entrainment occurs over the depth z of the buoyant element according to the entrainment hypothesis

$$\mu = \frac{1}{m(z)}\frac{\partial m(z)}{\partial z} \approx \frac{0.2}{r}, \qquad \text{(A.1)}$$

where μ is the total net fractional entrainment rate of the buoyant element, m its mass flux (m_u for updraft, m_d for downdraft), and r its radius. Following AS, the second part of this equation is not explicitly used. Implicitly, however, the radius of the cloud is assumed to be constant. Detrainment was originally only assumed to happen at the cloud top, but this assumption may easily be varied (Houze et al. 1979; Lord 1978) by defining a fractional detrainment rate μ_{ud} and rewriting (A.1) for the updraft as

$$\mu_u = \mu_{ue} - \mu_{ud} = \frac{1}{m_u(z)}\frac{\partial m_u(z)}{\partial z} = \frac{1}{m_u(\lambda, z)} \times \left\{\left[\frac{\partial m_u(\lambda, z)}{\partial z}\right]_{\text{ent}} - \left[\frac{\partial m_u(\lambda, z)}{\partial z}\right]_{\text{det}}\right\}, \qquad \text{(A.2)}$$

where λ characterizes the cloud type, μ_{ue} is the gross fractional entrainment rate, and μ_u the total net fractional entrainment rate of the updraft. Subscripts ent and det indicate changes due to entrainment and detrainment, respectively. Looking at the budget of a thermodynamic variable in an infinitesimal layer of the updraft, we get

$$\frac{\partial m_u \alpha_u}{\partial z} = \left(\frac{\partial m_u}{\partial z}\right)_e \tilde{\alpha} - \left(\frac{\partial m_u}{\partial z}\right)_d \alpha_u + S_u. \qquad \text{(A.3)}$$

Together with (A.2), this leads to the steady-state plume equation

$$\frac{\partial \alpha_u(\lambda, z)}{\partial z} = \mu_{ue}[\tilde{\alpha}(z) - \alpha_u(\lambda, z)] + S_u, \qquad \text{(A.4)}$$

where α is a thermodynamic variable, the tilde denotes an environmental value, and subscript u denotes an updraft property. Here, S stands for sources or sinks. Similarly, for the downdraft, we can rewrite Eqs. (A.2) and (A.4) as

$$\mu_d = \mu_{de} - \mu_{dd} = -\frac{1}{m_d(z)}\frac{\partial m_d(z)}{\partial z} = -\frac{1}{m_d(\lambda, z)}\left\{\left[\frac{\partial m_d(\lambda, z)}{\partial z}\right]_{\text{ent}} - \left[\frac{\partial m_d(\lambda, z)}{\partial z}\right]_{\text{det}}\right\} \qquad \text{(A.5)}$$

$$\frac{\partial \alpha_d(\lambda, z)}{\partial z} = -\mu_{de}[\tilde{\alpha}(z) - \alpha_d(\lambda, z)] + S, \qquad \text{(A.6)}$$

where subscript d denotes a downdraft property. For moist static energy

$$\tilde{h}(z) = C_p\tilde{T}(z) + gz + L\tilde{q}(z), \qquad \text{(A.7)}$$

Eqs. (A.4) and (A.6) simply become

$$\frac{\partial h_u(\lambda, z)}{\partial z} = \mu_{ue}[\tilde{h}(z) - h_u(\lambda, z)] \qquad \text{(A.8)}$$

and

$$\frac{\partial h_d(\lambda, z)}{\partial z} = -\mu_{de}[\tilde{h}(z) - h_d(\lambda, z)]. \qquad \text{(A.9)}$$

Next, for the moisture budget of the updraft, we use

$$\alpha_u = q_u(\lambda, z) + q_l(\lambda, z) \qquad \text{(A.10)}$$

and

$$S_u = -c_0 m_u(\lambda, z) q_l(\lambda, z). \qquad \text{(A.11)}$$

Here, S_u is the total water that is rained out, c_0 is a rainfall conversion parameter and could be a function of cloud size or wind shear, q_l is the suspended liquid water content of the cloud, and q_u is the water vapor mixing ratio inside the updraft. Equation (A.4) can then be rewritten as

$$\frac{\partial[q_u(\lambda, z) + q_l(\lambda, z)]}{\partial z} = \mu_{ue}[\tilde{q}(z) - q_u(\lambda, z) - q_l(\lambda, z)] + S_u. \qquad \text{(A.12)}$$

For the downdraft, the equation for the water vapor reads

$$\frac{\partial q_d(\lambda, z)}{\partial z} = -\mu_{de}[\tilde{q}(z) - q_d(\lambda, z)] + S_d. \quad \text{(A.13)}$$

Here, S_d is a source, namely, evaporation of rain. Assuming saturation in updraft and downdraft, we can make use of the approximate equation

$$q_c(\lambda, z) \approx \tilde{q}^* + \frac{\gamma}{1+\gamma}\frac{1}{L}[h_c(\lambda, z) - \tilde{h}^*(z)], \quad \text{(A.14)}$$

where

$$\gamma = \frac{L}{c_p}\left(\frac{\partial \tilde{q}^*}{\partial T}\right)_P \quad \text{(A.15)}$$

and h_c here stands for the moist static energy in the cloud (updraft or downdraft), if saturation is assumed to calculate S_u, S_d, and q_l. Next, to arrive at a usable closure, the up- and downdraft mass fluxes are normalized by the updraft base mass flux $[m_b(\lambda)]$ and the downdraft base mass flux $m_0(\lambda)$ of a subensemble. Hence, for the updraft,

$$m_u(\lambda, z) = m_b(\lambda)\eta_u(\lambda, z) \quad \text{(A.16)}$$

and

$$\mu_{ue} - \mu_{ud} = \frac{1}{\eta_u(\lambda, z)}\frac{\partial \eta_u(\lambda, z)}{\partial z}. \quad \text{(A.17)}$$

Equivalently, for the downdraft we may write

$$m_d(z) = m_0(\lambda)\eta_d(\lambda, z) \quad \text{(A.18)}$$

and

$$\mu_{de} - \mu_{dd} = \frac{1}{\eta_d(\lambda, z)}\frac{\partial \eta_d(\lambda, z)}{\partial z}. \quad \text{(A.19)}$$

Here, m_0 is the mass flux at the originating level and η_d, much as in equation (A.16), is the normalized mass-flux profile.

To leave only one unknown variable, we follow Houze et al. (1979) and make the originating mass flux of the downdraft a function of updraft mass flux and reevaporation of convective condensate. Therefore, the condensate in the updraft

$$C_u(\lambda)d\lambda = m_b d\lambda\left[\int_{z_B}^{z_T} \eta_u(\lambda, z)S_u dz\right] \equiv I_1 m_b d\lambda \quad \text{(A.20)}$$

is apportioned according to

$$C_u(\lambda)d\lambda = [R_c(\lambda) + E_d(\lambda)]d\lambda = [\alpha(\lambda) + \beta(\lambda)]C_u(\lambda)d\lambda, \quad \text{(A.21)}$$

where $\alpha + \beta = 1$ and E_d, the evaporation of condensate in the downdraft for cloud type λ can be written as

$$E_d d\lambda = m_0(\lambda)d\lambda\left[\int_0^{z_0} \eta_d(\lambda, z)S_d dz\right] \equiv I_2 m_0 d\lambda. \quad \text{(A.22)}$$

From Eqs. (A.20)–(A.22), we see that

$$E_d d\lambda = \beta C_u d\lambda = \beta I_1 m_b d\lambda = I_2 m_0 d\lambda, \quad \text{(A.23)}$$

and hence,

$$m_0(\lambda) = \frac{\beta(\lambda)I_1 m_b(\lambda)}{I_2(\lambda)} = \epsilon(\lambda)m_b(\lambda). \quad \text{(A.24)}$$

Here, $1 - \beta$ is the precipitation efficiency. Following Fritsch and Chappell (1980), it is made dependent on the wind shear.

To solve these equations, we need to specify boundary conditions as well as some arbitrary assumptions. For the updraft, we assume

$$h_u(z_b) = \max[\tilde{h}(z)], \quad \text{with} \quad z \leq z_b \quad \text{(A.25)}$$

$$h_u(\lambda, z_T) = \tilde{h}^*(z_T), \quad \text{(A.26)}$$

where the asterisk denotes a saturation value. Similarly, for the downdraft,

$$h_d(\lambda, z) = \min[\tilde{h}(z)]. \quad \text{(A.27)}$$

Physically, for both updraft and downdraft, we allow for maximum buoyancy. The boundary conditions for the updraft are different than in the original scheme, which had a rigid dependence on the PBL height. In the original scheme, the mixed layer was assumed to be well mixed and the cloud base was located on top of the mixed layer. In semiprognostic tests (Grell et al. 1991), large variations of moist static energy profiles were found in very low levels of the troposphere. This was caused by cold downdraft outflow. Naturally, the inflow to an updraft will not be a mixture of downdraft air and the more buoyant air; it is more likely the air with high, moist static energy from the layer above the downdraft outflow. Furthermore, compensatory subsidence should continue only to the level from which the updraft draws its air. Compensatory uplifting may be required in very low layers of the troposphere because of downdraft mass flux.

b. Feedback

The governing equations for the larger-scale environment were expressed in a convenient form (Schubert 1974) as

$$\rho\frac{\partial \bar{s}}{\partial t} + \nabla\cdot(\rho\bar{s}\mathbf{V}) + \frac{\partial \rho\bar{s}\bar{w}}{\partial z} = -\frac{\partial}{\partial z}F_{s-Ll} + LR + Q_R \quad \text{(A.28)}$$

$$\rho\frac{\partial \bar{q}}{\partial t} + \nabla\cdot(\rho\bar{q}\mathbf{V}) + \frac{\partial \rho\bar{q}\bar{w}}{\partial z} = -\frac{\partial}{\partial z}F_{q+l} - R, \quad \text{(A.29)}$$

where s is the dry static energy ($s = c_pT + gz$). The convective-scale fluxes are defined as

$$F_{s-Ll} \equiv F_s - LF_l \tag{A.30}$$

$$F_{q+l} \equiv F_q + F_l, \tag{A.31}$$

where F_s is the flux of dry static energy, F_q the flux of water vapor, and F_l the flux of suspended cloud liquid water. These are defined as

$$F_s(z) \equiv +\int_\lambda \eta_u(\lambda, z)[s_u(\lambda, z) - \bar{s}(z)]m_b(\lambda)d\lambda - \int_\lambda \eta_d(\lambda, z)[s_d(\lambda, z) - \bar{s}(z)]m_0(\lambda)d\lambda \tag{A.32}$$

$$F_q(z) \equiv +\int_\lambda \eta_u(\lambda, z)[q_u(\lambda, z) - \bar{q}(z)]m_b(\lambda)d\lambda - \int_\lambda \eta_d(\lambda, z)[q_d(\lambda, z) - \bar{q}(z)]m_0(\lambda)d\lambda \tag{A.33}$$

$$F_l(z) \equiv \int_\lambda \eta_u(\lambda, z)l(\lambda, z)m_b(\lambda)d\lambda. \tag{A.34}$$

The rainfall (convective-scale sink of cloud water) is defined as

$$R(z) \equiv +\int_\lambda \eta_u(\lambda, z)c_0(\lambda)l(\lambda, z)m_b(\lambda)d\lambda - \int_\lambda \eta_d(\lambda, z)q_e(\lambda, z)m_0(\lambda)d\lambda. \tag{A.35}$$

The second terms on the right-hand sides of Eqs. (A.32)–(A.35) are due to downdrafts and are zero above the downdraft-originating level. Below the updraft-air-originating level, the first terms of the right-hand sides are zero and only downdrafts affect the larger-scale environment. Below the updraft-air-originating level, the convective-scale fluxes due to updrafts are zero. Between the updraft-air-originating level and the level of free convection (the LFC), F_l and R are set to zero. Since no liquid water is assumed to be in the environment as the downdraft, the downward flux due to updrafts as well as downdraft fluxes in Eq. (A.33) are zero. Schubert (1974) showed that convection will not increase the total moist static energy per unit area in a column. In essence, only precipitation can change the dry static energy budget and the total mass of water vapor. All variables in the flux terms can be determined from the equations of the static control, except $m_b(\lambda)$. This is determined in the dynamic control, which incorporates the closure assumption of the scheme and is described next.

c. Dynamic control

Arakawa and Schubert first introduced the cloud work function, which is an integral measure of the buoyancy force associated with a subensemble. Starting with

$$\frac{dw_u}{dt} = B_u - F_r = \frac{dw_u}{dz}\frac{dz}{dt} = \frac{d}{dt}\frac{d}{dz}\frac{w_u^2}{2} = \frac{1}{w_u}\frac{d}{dt}\frac{w_u^2}{2}, \tag{A.36}$$

where B_u is the acceleration due to buoyancy and F_r the deceleration due to friction, multiplying Eq. (A.36) by $\rho_u(\lambda, z)w_u(\lambda, z)$ gives

$$\frac{d}{dt}\rho_u\frac{w_u^2}{2} = \rho_u w_u(B_u - F_r). \tag{A.37}$$

Integrating over the depth of the updraft and using $m_u = \rho_u w_u = m_b\eta_u$ yields

$$\frac{d}{dt}\int_{z_b}^{z_T}\rho_u\frac{w_u^2}{2}dz = m_b(\lambda)\int_{z_b}^{z_T}\eta_u B_u dz - D_u, \tag{A.38}$$

where D is the updraft-scale kinetic energy dissipation. Equation (A.38) can be written in the symbolic form

$$\frac{d}{dt}\overline{\mathrm{KE}}_u = A_u(\lambda)m_b(\lambda) - D_u(\lambda), \tag{A.39}$$

where $A_u(\lambda)$ is a measure of the efficiency of kinetic energy generation inside the cloud and is called the cloud work function. It can also be written as

$$A_u(\lambda) = \int_{z_B}^{z_T}\frac{g}{C_pT(z)}\frac{\eta_u(\lambda, z)}{1+\gamma}[h_u(\lambda, z) - \tilde{h}^*(z)]dz, \tag{A.40}$$

where γ is defined as in Eq. (A.15). Similar to Eqs. (A.36)–(A.38), defining a kinetic energy generation inside the downdraft leads to

$$\frac{d}{dt}\overline{\mathrm{KE}}_d = A_d(\lambda)m_0(\lambda) - D_d(\lambda), \tag{A.41}$$

where A_d, the measure of the efficiency of kinetic energy generation inside the downdraft, can be written as

$$A_d(\lambda) = \int_{z_0}^{z_{sur}}\frac{g}{C_pT(z)}\frac{\eta_d(\lambda, z)}{1+\gamma} \times [\tilde{h}^*(z) - h_d(\lambda, z)]dz. \tag{A.42}$$

Note that dry static energy instead of moist static energy would have to be used if subsaturation were assumed. We can combine Eqs. (A.39) and (A.40) and then make use of (A.24) to yield

$$\frac{d}{dt}\overline{\mathrm{KE}}_{\mathrm{tot}} = A_{\mathrm{tot}}(\lambda)m_b(\lambda) - D_{\mathrm{tot}}(\lambda), \tag{A.43}$$

where

$$A_{\text{tot}}(\lambda) = A_u(\lambda) + \epsilon(\lambda)A_d(\lambda) \qquad \text{(A.44)}$$

is the total cloud work function, which was redefined as a measure of the efficiency of kinetic energy generation in updraft as well as downdraft. Next, AS separated the change of the cloud work function into two parts: one is due to the change in the larger-scale variables,

$$\left(\frac{dA_{\text{tot}}}{dt}\right)_{\text{LS}} \equiv F(\lambda), \qquad \text{(A.45)}$$

and one is due to the modification of the environment by the clouds. Since the cumulus feedback on the larger-scale fields is a linear function of m_b, this term can be written in the symbolic form

$$\left(\frac{dA_{\text{tot}}}{dt}\right)_{\text{CU}} \equiv \int_\lambda K(\lambda, \lambda')m_b(\lambda')d\lambda. \qquad \text{(A.46)}$$

Therefore,

$$\frac{dA_{\text{tot}}}{dt} = F(\lambda) + \int_\lambda K(\lambda, \lambda')m_b(\lambda')d\lambda, \qquad \text{(A.47)}$$

where $K(\lambda, \lambda')$ are the kernels. The kernels are an expression for the interaction between clouds (updrafts and downdrafts). Equation (A.47) is solved with a linear programming method (Lord 1978), using various closures for dA_{tot}/dt as described in section 3.

In the original version of the Arakawa–Schubert scheme, the fractional entrainment rate was the parameter that characterized the cloud. In later papers, the cloud-top detrainment level was chosen instead. Assuming a fine vertical resolution, the second choice will most likely be better numerically, since no interpolation is necessary at the cloud tops. In the extremely unstable environment of the midlatitudes, however, it is sometimes impossible to calculate "clouds" with cloud tops in the unstable layers. Entrainment rates would have to be extremely large to stop cloud growth. In the experiments following, we therefore chose the original version, and used the fractional entrainment rate as the spectral parameter. For differences in the discretized equations, refer to appendix B.

APPENDIX B

Discretized Form of the Parameterization

Here, again we will focus on differences to Lord (1978), as well as downdraft discretization. In this study, the cloud base is a function of time and space. Note, however, that at a specific grid point the cloud base will be the same for every member of the subensemble. We also distinguish between an updraft-air-originating level, z_u, a downdraft-air-originating level, z_0, a cloud-base level, z_b (the LCL), and a level of free convection, z_{bc} (LFC). Here, z_u is determined from condition (A.25) and determines the thermodynamic properties of the updraft from cloud type i. The air becomes saturated at z_b; condensation will start, but no convection can occur yet, because the buoyancy is negative. In some instances this level could be the same as the LFC. The LFC is of great importance since this is the level at which the static control starts the calculations of individual convective elements. Since the air that feeds the cloud originates below the LCL, compensatory subsidence is allowed to reach the originating level of the updraft air.

For the downdraft, the originating level is also a function of time and space. If the downdraft exists, it will always reach the surface.

To be consistent with the discretized equations for the updraft, we define the mass budget for the downdraft in layer k as

$$e_d(k, i) - d_d(k, i) = \eta_d(k + 0.5, i) - \eta_d(k - 0.5, i), \qquad \text{(B.1)}$$

where entrainment and detrainment for the downdraft are defined as

$$e_d(k, i) = \mu_{de}\Delta z_d \eta_d(k - 0.5, i) \qquad \text{(B.2)}$$

and

$$d_d(k, i) = \mu_{dd}\Delta z_d \eta_d(k - 0.5, i). \qquad \text{(B.3)}$$

Combining these three equations yields

$$\eta_d(k + 0.5, i) = \eta_d(k - 0.5, i)(1 + \mu_{de}\Delta z_d - \mu_{dd}\Delta z_d). \qquad \text{(B.4)}$$

Here, we define $\Delta z_d = z(k + 0.5) - z(k - 0.5)$. The discretized form for the downdraft moist static energy budget reads

$$e_d(k, i)\tilde{h}(k) - d_d(k, i)\frac{h_d(k + 0.5, i) - h_d(k - 0.5, i)}{2} = \eta_d(k + 0.5, i)h_d(k + 0.5, i) - \eta_d(k - 0.5, i)h_d(k - 0.5, i). \qquad \text{(B.5)}$$

Using Eqs. (B.1)–(B.4) in Eq. (B.5) leads to

$$h_d(k + 0.5, i) = \frac{h_d(k - 0.5, i)(1.0 - 0.5\mu_{dd}\Delta z_d) + \mu_{de}\Delta z_d \tilde{h}(k)}{1 + \mu_{de}\Delta z_d - \mu_{dd}\Delta z_d + 0.5\mu_{dd}\Delta z_d}. \qquad \text{(B.6a)}$$

The moisture budget for the downdraft is developed in several steps. First, the downdraft water vapor mixing ratio before evaporation, but after entrainment, is calculated. This is done using

$$q_d(k, i) = \frac{q_d(k-0.5, i)(1-0.5\mu_{dd}\Delta z_d) + \mu_{de}\Delta z_d \tilde{q}(k)}{1 + \mu_{de}\Delta z_d - \mu_{dd}\Delta z_d + 0.5\mu_{dd}\Delta z_d}. \quad \text{(B.6b)}$$

Next, Eqs. (A.14) and (A.15) give the mixing ratio that the downdraft would have if saturated, q_{vd}. Hence, the amount of moisture that is necessary to keep the downdraft from cloud type i saturated in layer k is

$$q_e(k, i) = q_d(k, i) - q_{vd}(k, i). \quad \text{(B.7)}$$

Next, we check whether the updraft produces enough rain to sustain saturation in the downdraft by requiring that

$$\sum c_0 \Delta z(k) \eta_u(k-0.5, i) q_l(k-0.5, i) - \sum \epsilon(i) \Delta z(k) \eta_d(k+0.5, i) q_e(k, i) > 0. \quad \text{(B.8)}$$

If this is not the case, a downdraft is not allowed to exist.

Having defined the discretized versions of the equations from the static control, we now can describe the procedure.

Using the larger-scale temperature and moisture fields (T_0, q_0) at time t_0, and given a functional or empirical relationship for μ_d, μ_{de}, and μ_{dd}, the equations from the static control are used to calculate μ_{ue}, $h_u(z, i)$, $h_d(z, i)$, $q_u(z, i)$, $q_d(z, i)$, $\eta_u(z, i)$, and $\eta_d(z, i)$ for cloud type i. These are needed to determine the total cloud work function A_{tot} using

$$A_{\text{tot}}(i) = A_u(i) + \epsilon A_d(i). \quad \text{(B.9)}$$

The discretized versions of Eqs. (A.40) and (A.42) to determine the cloud work functions for updrafts and downdrafts are

$$A_u(i) = \sum_{k=\text{LFC}}^{k=\text{ktop}} \left\{ \frac{g}{c_p T(k-0.5)} \eta_u(k-0.5, i) \times \left[\frac{h_u(k-0.5, i) - \tilde{h}^*(k-0.5)}{1 + \gamma(k-0.5)} \right] \times [z(k-1) - z(k)] \right\} \quad \text{(B.10)}$$

and

$$A_d(i) = \sum_{k=z_0}^{k=\text{sur}} \left\{ \frac{g}{c_p T(k-0.5)} \eta_d(k-0.5, i) \times \left[\frac{h_d(k-0.5, i) - \tilde{h}^*(k-0.5)}{1 + \gamma(k-0.5)} \right] \times [z(k) - z(k-1)] \right\}. \quad \text{(B.11)}$$

The kernels of cloud type i are, by definition, the changes of the cloud work functions due to another subensemble, i'. Thus, following Lord (1978), T_0 and q_0 are modified by an arbitrary amount of mass flux, $m'_b \Delta t'$, from the i' subensemble. This is done for every possible subensemble and can be written in the symbolic form

$$\bar{T}'(k, i) = \bar{T}(k) + \delta_{i'}[\bar{T}(k)] m'_b \Delta t' \quad \text{(B.12)}$$

$$\bar{q}'(k, i) = \bar{q}(k) + \delta_{i'}[\bar{q}(k)] m'_b \Delta t'. \quad \text{(B.13)}$$

The δ terms, which are changes per unit $m_b(i)$, are easily calculated from budget considerations, as in Lord (1978). With the downdraft terms, the moist static energy budget of layer k and cloud type i becomes

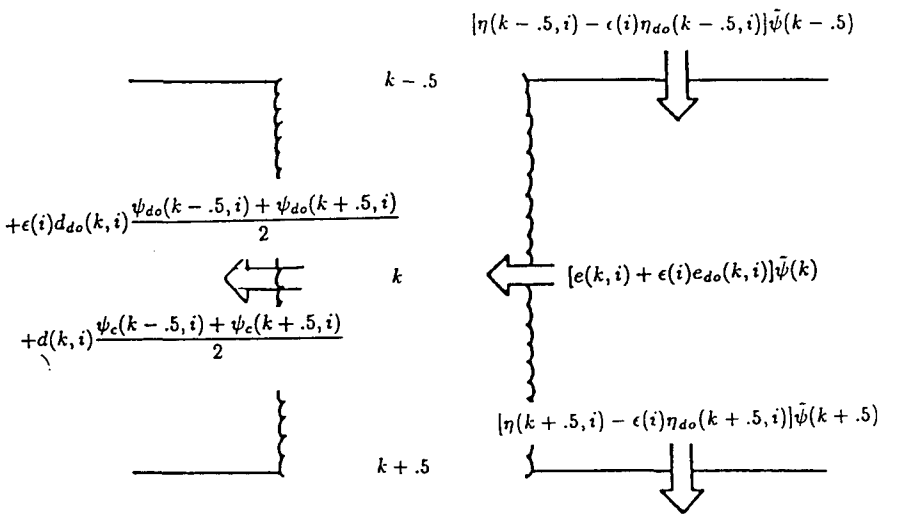

FIG. B1. Large-scale budget for variable ψ and layer k per unit mass of cloud type i.

$$\frac{\Delta p(k)}{g}\delta_{i'}[\tilde{h}(k,i)] = +[\eta_u(k-0.5,i) - \epsilon(i)\eta_d(k-0.5,i)]\tilde{h}(k-0.5)$$
$$-[\eta_u(k+0.5,i) - \epsilon(i)\eta_d(k+0.5,i)]\tilde{h}(k+0.5) - [e_u(k,i) + \epsilon(i)e_d(k,i)]\tilde{h}(k)$$
$$+ d_u(k,i)\frac{h_u(k+0.5,i) + h_u(k-0.5,i)}{2} + \epsilon(i)d_d(k,i)\frac{h_d(k+0.5,i) + h_d(k-0.5,i)}{2}, \quad \text{(B.14)}$$

where $e_u(k,i)$, $d_u(k,i)$, are entrainment and detrainment for the updraft, and $\Delta p(k)$ is defined by $\Delta p(k) = p(k+0.5) - p(k-0.5)$. A simple physical interpretation of the terms on the right-hand side can be understood by looking at Fig. B1. The first term is the subsidence on top of the layer, and the second is the subsidence on the bottom of the layer. This subsidence is an environmental compensatory mass flux due to the updraft and downdraft mass fluxes inside the cloud. Note that below z_u the "compensatory subsidence" may be compensatory uplifting, since in that case only downdrafts exist. The third term resembles entrainment into the updraft and downdraft; the fourth term resembles detrainment from the edges of the updraft; the fifth term resembles detrainment from the edges of the downdraft.

For the moisture budget,

$$\frac{\Delta p(k)}{g}\delta_{i'}[\tilde{q}(k,i)] = +[\eta_u(k-0.5,i) - \epsilon(i)\eta_d(k-0.5,i)]\tilde{q}(k-0.5)$$
$$-[\eta_u(k+0.5,i) - \epsilon(i)\eta_d(k+0.5,i)]\tilde{q}(k+0.5) - [e_u(k,i) + \epsilon(i)e_d(k,i)]\tilde{q}(k)$$
$$+ d_u(k,i)\frac{q_u(k+0.5,i) + q_u(k-0.5,i)}{2} + \epsilon(i)d_d(k,i)\frac{q_d(k+0.5,i) + q_d(k-0.5,i)}{2}. \quad \text{(B.15)}$$

At the cloud top, where downdrafts have no effects and updrafts detrain all their mass, Eqs. (B.14) and (B.15) read

$$\frac{\Delta p(\text{ktop})}{g}\delta_{i'}[\tilde{h}(\text{ktop},i)] = -\eta_u(\text{ktop}+0.5,i)\tilde{h}(\text{ktop}+0.5) - e_u(\text{ktop},i)\tilde{h}(\text{ktop})$$
$$+ d_u(\text{ktop},i)\frac{h_u(\text{ktop}+0.5,i) + h_u(\text{ktop},i)}{2} + \eta_u(\text{ktop},i)h_u(\text{ktop},i), \quad \text{(B.16)}$$

and

$$\frac{\Delta p(\text{ktop})}{g}\delta_{i'}[\tilde{q}(\text{ktop},i)] = -\eta_u(\text{ktop}+0.5,i)\tilde{q}(\text{ktop}+0.5) - e_u(\text{ktop},i)\tilde{q}(\text{ktop})$$
$$+ d_u(\text{ktop},i)\frac{q_u(\text{ktop}+0.5,i) + q_u(\text{ktop},i)}{2} + \eta_u(\text{ktop},i)q_u(\text{ktop},i). \quad \text{(B.17)}$$

Here, $\Delta p(\text{ktop}) = p(\text{ktop}+0.5) - p(\text{ktop}-0.5)$. Note that in the fourth term we have included the detrainment of all the cloud mass at the cloud top. Finally, at the surface (the downdraft tops) Eqs. (B.14) and (B.15) become

$$\frac{\Delta p(\text{ksur})}{g}\delta_{i'}[\tilde{h}(\text{ksur},i)] = -\epsilon(i)\eta_d(\text{ksur}-0.5,i)\tilde{h}(\text{ksur}-0.5) + \epsilon(i)\eta_d(\text{ksur},i)h_d(\text{ksur},i)$$
$$-\epsilon(i)e_d(\text{ksur}-0.5,i)\tilde{h}(\text{ksur}-0.5) + \epsilon(i)d_d(\text{ksur},i)\frac{h_d(\text{ksur},i) + h_d(\text{ksur}-0.5,i)}{2}, \quad \text{(B.18)}$$

and

$$\frac{\Delta p(\text{ksur})}{g}\delta_{i'}[\tilde{q}(\text{ksur},i)] = -\epsilon(i)\eta_d(\text{ksur}-0.5,i)\tilde{q}(\text{ksur}-0.5) + \epsilon(i)\eta_d(\text{ksur},i)q_d(\text{ksur},i)$$
$$-\epsilon(i)e_d(\text{ksur}-0.5,i)\tilde{q}(\text{ksur}-0.5) + \epsilon(i)d_d(\text{ksur},i)\frac{q_d(\text{ksur},i) + q_d(\text{ksur}-0.5,i)}{2}, \quad \text{(B.19)}$$

with $\Delta p(\text{ksur}) = p(\text{ksur} + 0.5) - p(\text{ksur} - 0.5)$. Here, the first term is the compensatory environmental mass flux, the second term is the detrainment of all downdraft air at the bottom, the third term is entrainment into the downdraft, and the fourth term is the detrainment of air around the downdraft edges.

The new thermodynamic fields, $T'_0(k, i')$ and $q'_0(k, i')$, are then used again from the static control to calculate new cloud properties and a new cloud work function, $A'_{\text{tot}}(i', i)$. Note that T'_0 and q'_0 are now functions of the subensemble i'. From the definition of the kernel, we then can calculate the kernels simply as

$$K(i, i') = \frac{A'_{\text{tot}}(i', i) - A_{\text{tot}}(i)}{m''_b \Delta t''}. \quad \text{(B.20)}$$

With this implicit way of calculating the kernels, the equations from the static control, which depend on the cloud model and are a separate entity in the code (a "black box"), can easily be modified or exchanged in order to use a more sophisticated cloud model. Note, however, that in such a case, Eqs. (B.14)–(B.19) may also need to be modified. Next, we go back to the original fields and modify those with the large-scale advective changes to get

$$T''(k) = T_0 + \left(\frac{\partial T}{\partial t}\right)_{\text{ADV}} \Delta t \quad \text{(B.21)}$$

and

$$q''(k) = q_0 + \left(\frac{\partial q}{\partial t}\right)_{\text{ADV}} \Delta t, \quad \text{(B.22)}$$

where (B.21) and (B.22) are applied over $\Delta t = 30$ min. The double prime quantities are then again used by the static control, which will calculate new cloud properties, and so new cloud work functions, $A''_{\text{tot}}(i)$, will be determined. Next the large-scale forcing—by definition, the change of the cloud work function due to large-scale effects only—is calculated using

$$F(i) = \frac{A''_{\text{tot}}(i) - A_{\text{tot}}(i)}{\Delta t}. \quad \text{(B.23)}$$

Note again that the advantage of this implicit way is that the static control may be easily altered. Furthermore, the accuracy of Eq. (B.23) could be improved by adding various terms to Eqs. (B.21) and (B.22), if closure is known or empiricism can be assumed. If downdrafts are included in the scheme, a dynamic effect of downdrafts for subsequent updrafts could be modeled as proposed by Frank and Cohen (1987) for their parameterization.

The large-scale forcing and the kernels are then both used by the dynamic control to estimate the cloud-base mass-flux distribution function m_b, using an IMSL (International Math and Statistics Library) subroutine to solve the linear programming problem. Finally, the feedback to the larger-scale environment is simply given by

$$\left[\frac{\partial T(k)}{\partial t}\right]_{\text{CU}} = \sum_{i'=1}^{i'_{\max}} \delta'_i [T(k)] m_b(i') \quad \text{(B.24)}$$

$$\left[\frac{\partial q(k)}{\partial t}\right]_{\text{CU}} = \sum_{i'=1}^{i'_{\max}} \delta'_i [q(k)] m_b(i'), \quad \text{(B.25)}$$

and the precipitation can be calculated using

$$P = \sum_{i'=1}^{i'_{\max}} \sum_{k=1}^{k=\text{ktop}} c_0 \Delta z(k) q_l(k + 0.5, i) m_u(k + 0.5, i) - \sum_{i'=1}^{i'_{\max}} \sum_{k=1}^{k=\text{ktop}} \Delta z(k) q_{ev}(k + 0.5, i) \times m_d(k + 0.5, i). \quad \text{(B.26)}$$

REFERENCES

Anthes, R. A., 1977: A cumulus parameterization scheme utilizing a one-dimensional cloud model. *Mon. Wea. Rev.*, **105,** 270–286.

——, E.-Y. Hsie, and Y. H. Kuo, 1987: Description of the Penn State/NCAR Mesoscale Model Version 4 (MM4). NCAR Tech. Rep., NCAR/TN-282+STR, 66 pp.

Arakawa, A., and W. H. Schubert, 1974: Interaction of a cumulus cloud ensemble with the large scale environment. Part I. *J. Atmos. Sci.*, **31,** 674–701.

Blackadar, A. K., 1979: High resolution models of the planetary boundary layer. *Advances in Environmental Science and Engineering,* 1, No. 1, J. Pfafflin and E. Ziegler, Eds., Gordon and Briech Scientific Publishing, 50–85.

Betts, A. K., 1974: The scientific basis and objectives of the U.S. subprogram for the GATE. *Bull. Amer. Meteor. Soc.*, **55,** 304–313.

Charney, J. G., and A. Eliassen, 1964: On the growth of the hurricane depression. *J. Atmos. Sci.*, **21,** 68–75.

Donner, L. J., 1993: A flux-momentum parameterization for cumulus convection: Vertical structures and mesoscale effects. *J. Atmos. Sci.*, **50,** in press.

Fraederich, K., 1973: On the parameterization of cumulus convection by lateral mixing and compensating subsidence. Part I. *J. Atmos. Sci.*, **30,** 408–413.

Frank, W. M., and C. Cohen, 1987: Simulation of tropical convective systems. Part I: A cumulus parameterization. *J. Atmos. Sci.*, **44,** 3787–3799.

Fritsch, J. M., and C. F. Chappel, 1980: Numerical prediction of convectively driven mesoscale pressure systems. Part I: Convective parameterization. *J. Atmos. Sci.*, **37,** 1722–1733.

——, C. F. Chappel, and L. R. Hoxit, 1976: The use of large-scale budgets for convective parameterization. *Mon. Wea. Rev.*, **104,** 1408–1418.

Grell, G. A., 1988: Semi-prognostic tests of cumulus parameterization schemes in the middle latitudes. Ph.D. dissertation, University of Miami, Coral Gables, Florida, 225 pp.

——, Y.-H. Kuo, and R. Pasch, 1991: Semiprognostic tests of cumulus parameterization schemes in the middle latitudes. *Mon. Wea. Rev.*, **119,** 5–31.

Houze, R. A., C.-P. Cheng, C. A. Leary, and J. F. Gamache, 1979: Diagnosis of cloud mass and heat fluxes from radar and synoptic data. *J. Atmos. Sci.*, **37,** 754–773.

Johnson, R. H., and P. J. Hamilton, 1988: The relationship of surface pressure features to the precipitation and airflow structure of an intense mid-latitude squall line. *Mon. Wea. Rev.*, **116,** 1444–1472.

Kain, J. S., and J. M. Fritsch, 1990: A one-dimensional entraining/detraining plume model and its application in convective parameterization. *J. Atmos. Sci.*, **47,** 2784–2802.

Kreitzberg, C. W., and D. J. Perkey, 1976: Release of potential instability: Part I. A sequential plume model within a hydrostatic primitive equation model. *J. Atmos. Sci.*, **33,** 456–475.

Krishnamurti, T. N., Y. Ramanathan, H.-L. Pan, R. J. Pasch, and J. Molinari, 1980: Cumulus parameterization and rainfall rates I. *Mon. Wea. Rev.*, **108,** 465–472.

——, S. Low-Nam, and R. Pasch, 1983: Cumulus parameterizations and rainfall rates II. *Mon. Wea. Rev.*, **111,** 815–828.

Kuo, H. L., 1965: On formation and intensification of tropical cyclones through latent heat release by cumulus convection. *J. Atmos. Sci.*, **22,** 40–63.

——, 1974: Further studies of the parameterization of the effect of cumulus convection on large scale flow. *J. Atmos. Sci.*, **31,** 1232–1240.

Kuo, Y.-H., and R. A. Anthes, 1984: Semi-prognostic tests of Kuo-type cumulus parameterization schemes in an extratropical convective system. *Mon. Wea. Rev.*, **112,** 1498–1509.

Lord, S., 1978: Development and observational verification of a cumulus cloud parameterization. Ph.D. dissertation, University of California, Los Angeles, 359 pp.

——, 1982: Interaction of a cumulus cloud ensemble with the large scale environment. Part III: Semi-prognostic test of the Arakawa–Schubert parameterization. *J. Atmos. Sci.*, **39,** 88–103.

Molinari, J., 1982: A method for calculating the effects of deep cumulus convection in numerical models. *Mon. Wea. Rev.*, **110,** 1527–1534.

——, and T. Corsetti, 1985: Incorporation of cloud-scale and mesoscale downdrafts into a cumulus parameterization: Results of one- and three-dimensional integrations. *Mon. Wea. Rev.*, **113,** 485–501.

Perkey, D. J., and C. W. Kreitzberg, 1976: A time-dependent lateral boundary scheme for limited area primitive equation models. *Mon. Wea. Rev.*, **104,** 744–755.

Rutledge, S. A., R. A. Houze, M. I. Biggerstaff, and T. Matejka, 1988: The Oklahoma–Kansas mesoscale convective system of 10–11 June 1985: Precipitation structure and single-Doppler radar analysis. *Mon. Wea. Rev.*, **116,** 1409–1430.

Schubert, W. H., 1974: Cumulus parameterization theory in terms of feedback and control. Colorado State University Atmospheric Science Technology Paper, No. 226, 19 pp.

Taylor, G. R., and M. B. Baker, 1987: A midlatitude cumulus parameterization that incorporates cloudtop entrainment. *Mon. Wea. Rev.*, **115,** 1173–1192.

Zhang, D.-L., 1989: The effect of parameterized ice microphysics on the simulation of vortex circulation with a mesoscale hydrostatic model. *Tellus*, **41A,** 132–147.

——, and K. Gao, 1989: Numerical simulation of an intense squall line during 10–11 June 1985 PRE-STORM. Part II: Rear inflow, surface pressure perturbations, and stratiform precipitation. *Mon. Wea. Rev.*, **117,** 2067–2094.

——, ——, and D. B. Parsons, 1989: Numerical simulation of an intense squall line during 10–11 June 1985 PRE-STORM. Part I: Model verification. *Mon. Wea. Rev.*, **117,** 960–994.